Energy Policy 203 (2025) 114618

Contents lists available at ScienceDirect

Energy Policy

journal homepage: www.elsevier.com/locate/enpol

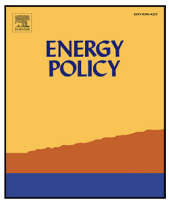

Research article

Smart Grid, Smart FiT: A data-driven approach to optimize microgrid energy market

Md. Ahasan Habib, M.J. Hossain *

School of Electrical and Data Engineering, University of Technology Sydney, Ultimo, 2007, NSW, Australia

ARTICLE INFO

Keywords:
Dynamic feed-in tariff
Sequential Model-Based Optimization
Data-driven energy pricing
PV generation

ABSTRACT

The dynamic nature of renewable energy production and customer demand necessitates a flexible approach for designing Feed-in Tariff (FiT) schemes to ensure equity and fairness. This research presents a comprehensive data-driven framework for determining FiT rates by analyzing trends in demand, renewable energy generation, and temperature over time. The proposed method calculates FiT rates that adapt dynamically to evolving scenarios by incorporating both historical and projected trends. To optimize FiT values and offer affordable tariffs beneficial to both energy providers and customers, the proposed approach employs Sequential Model-Based Optimization (SMBO). Case studies using real-world microgrid data showcase the model's adaptability and confirm its reliability by ensuring that the optimized FiT values remain within Australian government-set tariff limits. The SMBO method can decrease computational time by as much as 90%, achieving a Root Mean Square Error of 2.839. Additionally, the dynamic FiT model enhances financial sustainability by shortening the payback period for various prosumers by 17%–22% compared to a fixed FiT. The dynamic FiT adjusts rates based on previous historical and projected trends, incentivizing prosumers to export energy during peak demand. This method supports sustainable energy usage and offers a flexible, efficient pricing mechanism that adapts to the changing energy landscape.

1. Introduction

In light of the pressing climate change and energy security issues, the shift towards renewable energy sources has become necessary for both developed and middle-income nations. To achieve the targets outlined in the Sustainable Development Goals (SDGs), governments across the globe are placing a growing emphasis on sustainable energy solutions (Trends, 2017). A key strategy in this transition is promoting Distributed Energy Resources (DER), such as solar, wind, and other household-level renewable technologies. Government policies aim to decentralize energy production, cut greenhouse gas emissions, and enhance energy resilience by encouraging residents to install these systems. In addition to the vital role of establishing large-scale green energy facilities in this transition, governments also acknowledge the significance of involving households and businesses of all sizes in this journey. For instance, Australia has launched Project Edge, a 28 million-dollar initiative with support from the Australian Renewable Energy Agency (ARENA) (Victorian, 2024). This project aims to establish a DER marketplace in the Hume region of Victoria where users of DER systems from residential, commercial, and industrial sectors can trade electricity and grid services. China also heavily invests in DER projects to minimize carbon emissions and promote renewable energy. A notable endeavor is the Whole County PV program, which aims to install photovoltaics in rural areas (China, 2024). A major project, Tengger Desert, aims to create solar and wind power in arid locations (Lewis, 2023). In 2023, China added a record 217 GW of solar power, sustaining its leadership in renewable energy (Carbonbrief, 2024). Till August 2024, India was also able to contribute 46% of total energy from non-fossil fuel-based sources (India, 2024). This global momentum signifies a unified endeavor by both developed and developing countries to augment the share of renewable energy in their total energy composition.

Governments understand they cannot tackle this enormous challenge alone, so they offer industries and citizens appealing incentives to invest in renewable energy. For example, the Business Energy Investment Tax Credit (ITC) is a federal tax credit available in the United States that allows businesses to get up to a 26% tax credit for qualifying renewable energy projects (Federal, 2024). European nations use various government assistance systems to encourage renewable energy growth, such as FiT, Feed-in Premiums (FiP), and quota commitments with marketable green credits (Europe, 2024). They also give investment grants, tax incentives, and soft loans to promote renewable

* Corresponding author.
E-mail address: jahangir.hossain@uts.edu.au (M.J. Hossain).

https://doi.org/10.1016/j.enpol.2025.114618
Received 18 November 2024; Received in revised form 27 February 2025; Accepted 24 March 2025
Available online 9 April 2025

energy technology investment. Furthermore, the United Kingdom and Australian governments provide programs like the Smart Export Guarantee (SEG) (UKofgem, 2024) and small-scale technology certificates (STC) (AUScer, 2024) to encourage households and small enterprises to engage in renewable energy efforts. The government and energy providers offer programs that encourage households, or prosumers, to engage in the energy market. FiT is one of the most common and straightforward methods for buying and selling green energy between energy providers and prosumers, and it is widely used in various countries to promote renewable energy adoption.

There are numerous methods for determining the FiT for renewable energy exports. A common approach is cost-based modeling, where the FiT is set based on the expenses of renewable energy generation, including capital investment, operating costs, maintenance, and the levelized cost of electricity (LCOE) (Sener and Fthenakis, 2014; Gholami and Nils Røstvik, 2021). Additionally, depreciation, decommissioning costs, and compliance with regulatory policies also play a role in determining the overall tariff. Hafiz et al. proposed a FiT mechanism for European countries that used the LCOE of building-integrated PV systems in the capitals of member states, Norway, and Switzerland to determine appropriate subsidies or incentives (Gholami and Nils Røstvik, 2021). Wang et al. evaluated the economic performance of 24 microgrids using metrics such as net present value (NPV), economies of scale, and life-cycle cost (Wang et al., 2020). The purpose of the investigation is to offer policy recommendations to support renewable energy efforts in the near future and to provide generic insights into the economic viability of microgrids. K. Sagulpongmalee et al. suggested adopting FiT with three policy phases across the project lifespan to promote renewable energy development in Thailand (Sagulpongmalee et al., 2019). The authors calculated the FiT rate using NPV, IRR, benefit-cost ratio, and payback time. The FiT is initially initialized at a high fixed rate in the proposed model and is subsequently adjusted according to the system's degradation rate. Lastly, once the PV system reaches its goal, the auction procedure decides the tariff. The policy seems optimistic, but investors may doubt their ability to generate profitable returns. An NPV-based FiT was proposed in Poland (Górnowicz and Castro, 2020), while Ref. Li et al. (2021) applied a payback period approach to determine FiT in Australia. M. A. Kabir et al. utilized NPV, payback time, and profitability index to calculate FiT for PV exports at the industrial level in Bangladesh (Kabir et al., 2023). However, the calculated FiT by considering NPV is not reliable due to the volatility of interest rates (Dobrowolski and Drozdowski, 2022). Moreover, depending on IRR or payback period-based Fixed FiT over the project life cycle is tricky, as technology costs constantly change and monetary values regularly vary. It is challenging to achieve consistent returns over time due to these factors.

Several researchers have emphasized the impact of socioeconomic conditions, age, and income levels on the effectiveness and adoption of FiT in different regions. For example, K. Feng et al. found that elderly and low-income Australians are more inclined to install solar PV systems to receive incentives by exporting excess energy to grids (Feng et al., 2023). These specific groups installed more solar PV systems because the subsidies were tailored to benefit them. According to one study conducted in Japan, low-income households have a greater cost burden for PV system installation than others (Nagata et al., 2018). The authors contended that the equal FiT for all income levels raises questions regarding justice and equity. Similar types of research have been conducted in the UK, and the authors of Ref. Sovacool et al. (2022) pointed out four different types of inequities faced by the residents. Research from Germany (Hackbarth and Löbbe, 2020) and the United Kingdom (Balta-Ozkan et al., 2021) suggests that factors such as the desire for stronger social connections or greater energy independence may influence participation in renewable energy programs. For each distinct set of inhabitants, these reasons may be different. That means that people's financial situation, social ties, or personal goals all play a role in their decision to adopt renewable energy, making it important to consider these differences when designing FiT rates. Although these studies offer valuable insights into the impact of demographics and socioeconomic variables on FiT policies, developing a universal FiT calculation policy remains difficult. A one-size-fits-all FiT framework is challenging since individual behaviors, attitudes, and lifestyle choices are different and context-dependent (Yang and Matsumoto, 2023).

In many nations, including Australia, electricity consumption is priced based on demand and supply, but prosumers receive fixed FiTs for surplus energy. This fixed FiT model does not reflect the dynamic nature of electricity markets, where prices can change throughout the day owing to peak demand, weather, and grid load. Therefore, the static FiT strategy may limit financial incentives' ability to promote prosumers' optimal energy generation and consumption. In response to the challenges of fixed FiTs, dynamic FiT models have been developed to accommodate changing generation patterns and technological progress. L. Li et al. developed a dynamic FiT for an offshore wind farm in China, spanning ten years, to account for uncertainties in renewable intermittency and technology learning, ensuring optimal installed capacity at minimal policy cost (Li et al., 2020). The least squares Monte Carlo method and binary tree scenario generation determine ideal FIT levels. This work assumes that a certain amount of wind capacity will be added to the whole network, and the results reveal that the FiT has been falling over the last ten years. Despite the authors' claims of dynamic FiT, they provide one FiT rate for each year, regardless of generating or consumption patterns. According to Ref. Alizamir et al. (2016), market dynamics, learning and diffusion rates, and strategic investor behavior are all crucial aspects in the design of dynamic FiT. The authors claim that addressing these issues can prevent investors from delaying their investments, optimizing their adoption time and effectiveness of renewable energy. A mixed integer linear programming-based dynamic feed-in tariff is proposed in Selinger-Lutz et al. (2020) to maximize electricity sales profitability and thermal demand in a micro-combined heat and power plant. This strategy uses a rolling horizon technique to adjust a dynamic two-step tariff to daily market prices, boosting load shifting to high power rates. The authors of Yang and Ge (2018) introduced a dynamic FIT model that adjusts tariffs based on the decreasing costs of PV equipment. A new FiT model is proposed for Ukrainian households that modify export rates according to various economic, social, and environmental factors, promoting a well-rounded growth of renewable energy (Kurbatova et al., 2023). In Seyedzahedi and Bahramara (2023), the authors proposed a time-of-use (TOU) FiT structure in place of fixed FiT in Iran for promoting investments in PV systems.

Investment strategies in DER are subject to substantial variation worldwide as a result of variations in economic conditions, environmental objectives, cultural norms, and social structures. Renewable technologies, including solar PV and wind, are promoted by countries through the implementation of customized strategies, which may include market-driven pricing models and generous subsidies. China's recent FiT regulations have played a crucial role in driving renewable energy (RE) investment, but they also face significant limitations. While fixed FiT policies initially accelerated solar market growth, their rigid structure and rapid tariff reductions led to inefficiencies. According to Lin and Xie, RE investment increased nearly 3.4 times for every unit rise in subsidies (Lin and Xie, 2024). However, analysis shows that the current policy (2014–2021) primarily benefits large-scale RE producers. Additionally, Ref. Zhang et al. (2022) highlights that the fixed FiT policy fails to address regional disparities between areas with high solar potential and those with greater energy demand. Lin and Chen identify similar challenges hindering RE expansion in China (Lin and Chen, 2023). They propose region-specific FiTs that consider resource distribution, ensuring appropriate support levels to drive innovation. Furthermore, Ref. Auffhammer et al. (2021) suggests that transforming provincial electricity markets into interconnected regional markets could overcome interprovincial barriers, improving resource allocation and encouraging greater RE adoption.

FiT policies across Asia and Europe vary based on economic conditions, market dynamics, and consumer adoption capacity, leading to differing success levels and challenges in renewable energy integration. For example, P. Dato et al. found that Hong Kong's fixed FiT system fails to provide sufficient financial incentives for small-scale solar PV adoption, with payback periods reaching 50 years—exceeding PV panel lifespans (Dato et al., 2021). The break-even FiT rate predicted by the authors surpasses the government's fixed FiT, making it unsustainable over time. Two major challenges of the fixed FiT model are rising subsidy debt (from ¥ 19 billion in 2014 to ¥ 293 billion in 2019) and high curtailment rates, with up to 43% of wind power and 32% of solar PV wasted in northern China. According to Ref. Cai et al. (2024), households with battery storage face payback periods more than twice as long as those without, discouraging energy storage adoption. The study also suggests that households exceeding their daily PV generation capacity should increase self-consumption to ensure profitability, inadvertently discouraging further green energy expansion.

FiT implementation timing also affects PV system adoption. Kimura et al. found that Japan's high FiT rates, introduced without strict project deadlines, allowed developers to delay construction while securing inflated tariffs. This resulted in higher capital costs and slower cost reductions (Kimura et al., 2025). The study recommends linking FiT rates to market conditions at the time of project commissioning rather than approval to enhance cost efficiency and reduce financial strain. Similarly, Ref. le Maitre (2024) examines the impact of financial mechanisms on onshore wind energy in Germany, Denmark, the UK, and Ireland. While auctions and other market-driven approaches have increased deployment, they have disadvantaged small-scale community projects by limiting financial accessibility due to lower subsidies. The authors suggest balancing cost-efficiency with flexible funding schemes to promote community ownership and public support for RE expansion.

Vietnam's fixed FiT policy propelled it to become the world's third-largest solar market by 2020 but also introduced significant challenges (Le et al., 2022). Uniform FiT rates failed to align with regional LCOE, leading to uneven solar adoption. Sudden policy shifts triggered rushed project deployments, grid congestion, and investor uncertainty, underscoring the need for a more flexible, market-driven approach. Additionally, Ref. Azhgaliyeva et al. (2024) highlights that Vietnam's FiT policy prioritized solar over wind, biomass, and hydro, creating an imbalance in RE development. Malaysia's FiT system successfully advanced renewable energy adoption but lacked flexibility, leading to oversupply and inconsistencies with declining technology costs (Azhgaliyeva et al., 2024; Ravichandran and Selvaraj, 2021). In Thailand, FiT incentives disproportionately favored smaller firms over larger companies, reducing overall investment efficiency (Azhgaliyeva et al., 2024). These cases illustrate the necessity for adaptable FiT models that can respond to evolving market conditions and drive sustainable energy growth.

This research focuses on Australia, one of the leading green energy producers. The latest reports from the Clean Energy Council estimate that as of 2024, renewable sources contribute nearly 40% of Australia's total electricity supply with wind 13.4%, solar 18.2%, and hydro 6.5% (Clean Energy Council, 2024). Many states initially implemented high, government-backed FiTs to encourage investment in solar PV, such as New South Wales' Solar Bonus Scheme, which provided up to 60c/kWh (nswparliament, 2024). However, the government has since cut this offer. In the same vein, the Solar Bonus Scheme in Queensland has now closed to new applicants, and Tasmania has experienced a substantial decrease in its net FiT rates, which have decreased from 27.8c/kWh to 8.541c/kWh (Australian energy council, 2024). Additionally, the Renewable Energy Buyback Scheme in Western Australia, which offered 47c/kWh, has been phased away (Australian energy council, 2024). The decreasing financial incentives for solar PV installations are brought to light by these changes in FiT rates across the country. This further emphasizes the necessity for persistent and adaptive governmental support to encourage the use of renewable energy sources. Recent research in Ref. Zhang et al. (2021), Castaneda et al. (2020) and Ma et al. (2021) has demonstrated that lowering FiTs can lead to a decrease in household solar PV installations, thus delaying the transition to a low-carbon future. Lower FiTs may encourage the use of battery storage, but it is unclear how they will affect the overall adoption of renewable energy. Thus, it is necessary to carefully analyze FiT policies' long-term effects and investigate more flexible and dynamic ways to promote sustainable energy production. In the literature, it has been observed that fixed FiT models frequently encounter difficulty in keeping up with the rapid tempo of technological advancements, changing investment trends, and evolving government policies over extended periods of time (10–25 years). This lack of flexibility can cause financial losses for both electricity distributors and consumers, especially during periods of market instability.

As renewable energy systems continue to expand, policymakers are increasingly contemplating the implementation of dynamic and adaptable FiT structures to align energy tariffs with real-time supply and demand more effectively. One potential solution is the use of VPPs or virtual power plants (VPP, 2024). These combine several decentralized energy sources, such as solar panels and battery storage, into one flexible grid resource. New Australian regulations are planned to include dynamic FiT schemes that reflect market variations and encourage energy generation and use during peak demand. The goal of these policies is to lessen reliance on fossil fuels and improve grid stability by encouraging consumers to maximize energy output and sell excess power back to the grid when it is needed. Future FiT policies will better promote a decentralized, low-carbon energy system by instituting tariffs tied to real-time grid conditions and energy demand predictions. Dynamic models will assist policymakers in balancing renewable energy uptake, grid dependability, and energy producer compensation. To overcome these obstacles, this study suggests a data-driven architecture that dynamically modifies FiT rates in response to current trends in energy generation, consumption, and environmental conditions. This strategy has several benefits, including the ability to react in real-time, incentives for optimal behavior, promotion of grid stability, and assurance of fairness and equity. The key contributions of this research are given below:

- The proposed architecture provides an adaptive FiT calculation method that continuously adjusts tariffs in response to real-time changes in demand, temperature, and PV generation, ensuring seamless alignment with energy consumption patterns and renewable energy production.
- This method integrates both historical and projected trends, along with prior volatility, to capture long-term patterns while dynamically adapting to short-term fluctuations, resulting in a balanced and flexible tariff computation strategy.
- SMBO optimizes key input factor weights to calibrate FiT values for enhanced model flexibility and performance across various scenarios.
- The framework offers rapid computational performance, making it highly suitable for real-time decision-making in dynamic energy markets.

2. Proposed methodology

This section describes a data-driven, robust, and flexible FiT system for exporting PV generation to the utility grid. The overall framework of the proposed technique is represented in Fig. 1. The methodology uses historical and forecasted data on electricity demand, PV generation, and meteorological conditions to uncover significant temporal patterns. In this research, "exports" specifically refer to renewable energy—either fully generated or surplus—transmitted to the local grid, excluding cross-border electricity trades. The dynamic FiT framework applies only to energy fed into the domestic distribution network by prosumers. Other forms of electricity commerce, such as international

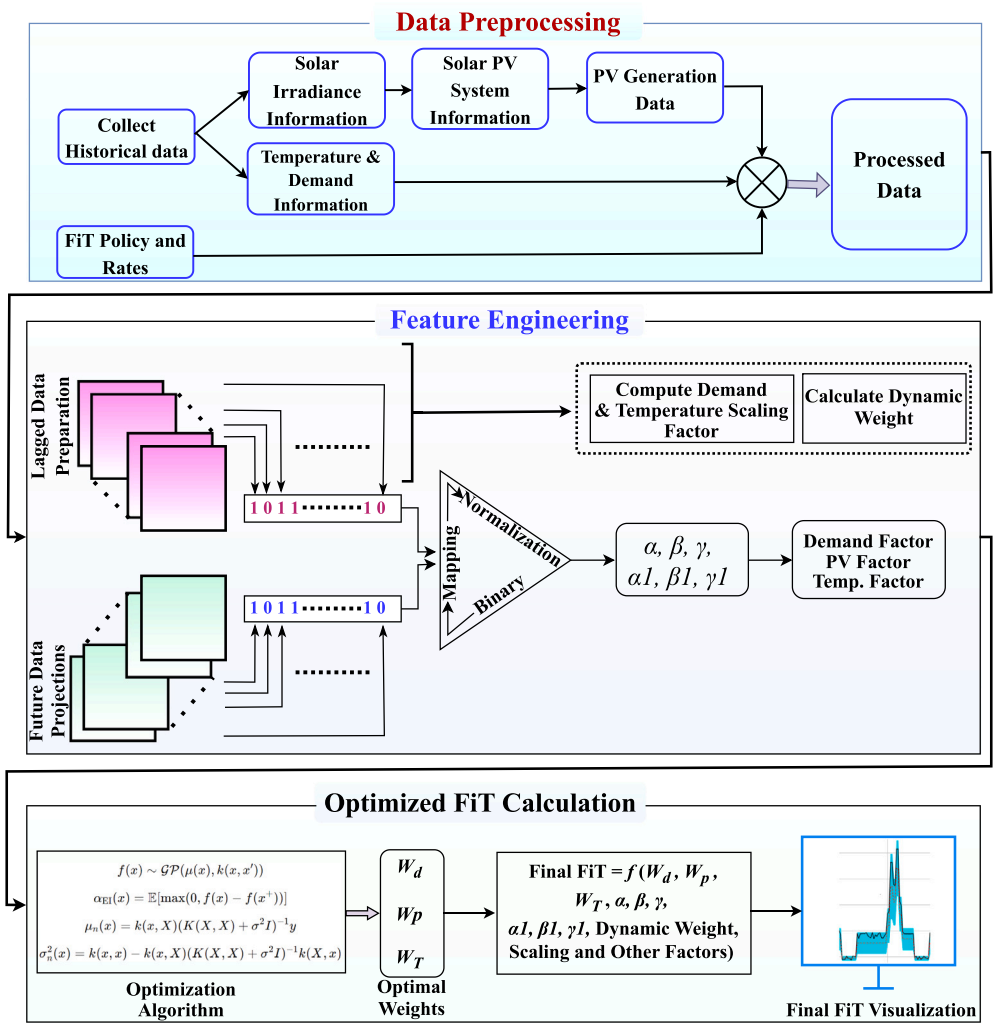

Fig. 1. Detailed methodological approach for FiT algorithm design and optimization.

exports, are beyond the scope of this study. The initial step involves collecting comprehensive past and future data, such as temperature, solar irradiance, solar PV system specifications, and demand data, as well as the current FiT rates and regulations. The data pre-processing phase cleans and handles missing values to produce a regional PV generation, demand, and temperature dataset. The following phase generates the necessary features, weights, and factors for calculating the final FiT.

In the second phase, temperature, demand, and PV generation data are organized by time, including historical and forecasted values. Binary encoding is applied to capture past and future trends in demand, PV generation, and temperature. Each binary pattern reflects the increase or decrease over specific time ranges. These binary patterns are later transformed into weighted factors for the final FiT formula. Past temperature and demand values are used to calculate scaling factors that show how current values compare to their maximum and minimum levels over the previous day. A dynamic weight term is also introduced to account for demand volatility, reflecting recent fluctuations. In the final stage, the SMBO method is used to determine the optimal weights for past and future input factors. The subsequent text provides a comprehensive explanation of the functions and mathematical expressions of each section. In the last stage, the SMBO algorithm is applied to evaluate the optimal weights for the past and future input factors. The following discussion explains the parts with extensive mathematical expressions and the functions of each section.

2.1. Data shifting, scaling, and factorization

The first stage is to shift the data for Demand, PV generation, and Temperature over different time periods in both past and future horizons. The shifted data can be expressed as follows:

$$X_{past} = \{x \in \{D, PV, T\} \mid x(t) = x(t-n),\ n \in \mathbb{Z}^+\} \tag{1}$$

$$X_{future} = \{x \in \{D, PV, T\} \mid x(t) = x(t+k),\ k \in \mathbb{Z}^+\} \tag{2}$$

where D, PV, and T denote Demand, PV generation, and Temperature, respectively. In addition, n and k represent the number of time steps in past and future, respectively. Next, rolling maximum and minimum values are calculated for each variable over a given window of time steps. Rolling maximum and minimum values depict trough behavior in a brief time frame and reveal imminent patterns and variations. These values are computed as:

$$R_{max}(X) = \max\left(X(t), X(t-1), \ldots, X(t-n)\right), \quad X \in \{D, PV, T\} \tag{3}$$

$$R_{min}(X) = \min\left(X(t), X(t-1), \ldots, X(t-n)\right), \quad X \in \{D, PV, T\} \tag{4}$$

Upon computing the rolling maximum and minimum values, scaling factors (S_X) for D and T are employed to assess the proximity of the present values to these extremes. Values approaching these thresholds indicate extreme conditions, such as high demand or severe temperature, triggering the FiT to modify rates. If the values surpass

specific criteria, (S_X) proliferates; otherwise, it changes gradually. The mathematical formula to calculate this scaling factor is described later. After calculating scaling factors, binary sequences are produced to monitor trends in demand, PV generation, and temperature. Each bit in the sequence evaluates the present sample against a preceding or subsequent value to ascertain whether the variable is ascending or descending. The binary patterns are combined with the position-wise weighted factors to produce six terms: $\alpha(t)$, $\beta(t)$, $\gamma(t)$, $\alpha_1(t)$, $\beta_1(t)$, and $\gamma_1(t)$. Here, $\alpha(t)$, $\beta(t)$, $\gamma(t)$ are for assigned to generate the coefficient for the past values of D, PV, T, respectively, and $\alpha_1(t)$, $\beta_1(t)$, $\gamma_1(t)$ represent the FiT coefficient of future values of three inputs. The mathematical expressions of the past and future trends extraction coefficients are given below:

$$Y(t) = \frac{\sum_{i=1}^{n} \left[B_Y(t-i, t-(i+1)) \cdot C_Y(i)\right]}{\sum_{i=1}^{n} C_Y(i)} \cdot \sigma(Y(t), \Delta_Y), \quad Y \in \{\alpha, \beta, \gamma\} \quad (5)$$

$$Y_1(t) = \frac{\sum_{j=1}^{m} \left[B_{Y_1}(t+j, t+(j-1)) \cdot C_{Y_1}(j)\right]}{\sum_{j=1}^{m} C_{Y_1}(j)} \cdot \sigma(Y_1(t), \Delta_{Y_1}), \quad Y_1 \in \{\alpha_1, \beta_1, \gamma_1\} \quad (6)$$

For each variable $Y \in \{\alpha, \beta, \gamma\}$, the binary digits $B_Y(t-i, t-(i+1))$ and $B_{Y_1}(t+j, t+(j-1))$ are generated by comparing each value with its preceding sample in both past and future sequences. The coefficients $C_Y(i)$ and $C_{Y_1}(j)$ correspond to the past and future time steps, respectively, adjusting the influence of each variable. The function $\sigma(Y(t), \Delta_Y)$ determines the sign adjustment for each variable based on thresholds(Th):

$$\sigma(Y(t), \Delta_Y) = \begin{cases} 1 & \text{if } Y(t) \geq Th_{\text{high}} \\ \rho & \text{if } Th_{\text{mid}} \leq Y(t) < Th_{\text{high}} \\ \pm\sigma & \text{if } Y(t) < Th_{\text{mid}} \end{cases} \quad (7)$$

The value $\pm\sigma$ depends on the trend direction, with $\Delta_Y = 1$ for an increasing trend and $\Delta_Y = -1$ for a decreasing trend.

2.2. Fit model formulation, optimization and evaluation

The FiT value at time t is calculated as a combination of three main components. These components are:

$$\text{FiT}(t) = \text{PTC}(t) + \text{CIS}(t) + \text{DRA}(t) \quad (8)$$

where PTC(t) represents the Primary Trend Contribution, CIS(t) stands for the Contextual Influence Scaling, and DRA(t) denotes the Dynamic Risk Adaptation. The following sections will explain the mathematical equations governing each component and their role in determining the overall FiT value.

2.3. Primary Trend Contribution (PTC)

The PTC captures the core influence of system trends and contributes the dominant share of the final FiT. The mathematical expression of computing this part is:

$$\text{PTC}(t) = Fit_{min} + a \cdot Fit_{diff} \cdot \left[\mathcal{I}_{\text{past}}(t) + \mathcal{I}_{\text{future}}(t)\right] \quad (9)$$

where the term a represents the weight assigned to the combined influence of past and future trends through $\mathcal{I}_{\text{past}}(t)$ and $\mathcal{I}_{\text{future}}(t)$ respectively. The formula to compute the $\mathcal{I}_{\text{past}}(t)$ and $\mathcal{I}_{\text{future}}(t)$ are defined as follows:

$$\mathcal{I}_{\text{past}}(t) = \sum_{Y \in \{\alpha, \beta, \gamma\}} Y \cdot \mathcal{W}_Y \cdot \sum_{X \in \{D, PV, T\}} \frac{X(t)}{R_{\max}(X)} \quad (10)$$

$$\mathcal{I}_{\text{future}}(t) = \sum_{Y_1 \in \{\alpha_1, \beta_1, \gamma_1\}} Y_1 \cdot \mathcal{W}_{Y_1} \cdot \sum_{X \in \{D, PV, T\}} \frac{X(t)}{R_{\max}(X)} \quad (11)$$

Table 1
Effect of past and future trends of D, PV, and T on α, β, γ and $\alpha_1, \beta_1, \gamma_1$ coefficients with PV.

P-D	P-PV	P-T	F-D	F-PV	F-T	α	β	γ	α_1	β_1	γ_1
↑	↑	↑	↑	↓	↑	+	+	+	+	−	+
↓	↓	↑	↑	↑	↓	−	−	+	+	+	−
↑	↓	↓	↓	↑	↑	+	+	−	−	+	+
↑	↑	↑	↑	↑	↑	+	+	+	−	+	+
↓	↓	↓	↓	↓	↓	−	−	−	+	−	−
↑	↓	↑	↑	↓	↑	+	+	+	+	−	+
↓	↑	↓	↓	↑	↓	−	+	−	−	+	−
↑	↑	↓	↑	↑	↓	+	+	−	+	+	−
↓	↓	↑	↓	↓	↑	−	−	+	−	−	+
C	**C**	**C**	**C**	**C**	**C**	**P**	**P**	**P**	**P**	**P**	**P**

P-D = Past Demand, P-PV = Past PV, P-T = Past Temperature, F-D = Future Demand, F-PV = Future PV, F-T = Future Temperature, C = Constant, P = Previous.

Table 2
Effect of past and future trends of D and T on past) and future coefficients for less or no PV power.

P-D	P-T	F-D	F-T	α	γ	α_1	γ_1
↑	↑	↑	↑	+	+	+	+
↓	↓	↓	↓	−	−	−	−
↑	↑	↑	↓	+	+	+	−
↓	↓	↓	↑	−	−	−	+
↑	↓	↑	↑	+	−	+	+
↓	↑	↓	↓	−	+	−	−
↑	↑	↓	↑	+	+	−	+
↓	↓	↑	↓	−	−	+	−
C	**C**	**C**	**C**	**P**	**P**	**P**	**P**

Here, $\mathcal{W}_Y(i)$ and $\mathcal{W}_{Y_1}(j)$ are the dynamic weight functions applied to the past and future contributions of $Y \in \{\alpha, \beta, \gamma\}$, respectively, to adjust the impact of each input variable over time.

Depending on whether X is increasing or decreasing, the trend detection coefficients for past and future values dynamically modify the contribution of each variable. Table 1 presents the coefficient's impact for various trend scenarios with PV generation. Row 1 indicates that the coefficients α and α_1 exhibit positive signs when both past and future demand are rising while future PV generation is declining. In response to the anticipated surge in demand, the FiT will be raised, incentivizing exports to meet the demand. On the other hand, when demand is on a declining trend from past to future (Row 7) and past and future PV generation increase, the coefficients β and β_1 take positive signs to reflect favorable PV conditions. At the same time, α and β_1 are assigned negative signs to discourage exports due to low demand. Similarly, Table 2 illustrates the past and future coefficient effects on FiT for low or no solar power generation. The coefficients indicate positive values when both temperature and demand exhibit increasing trends in the past and the future. This situation encourages exports to manage rising temperatures and demand (Row 1) and vice versa because of the reverse rationale (Row 2). When future demand falls, but the temperature rises (Row 7), the coefficients adjust for the lower future demand. The PTC component synchronizes the FiT accurately according to the trends of alterations in past and future values.

2.4. Contextual Influence Scaling (CIS)

Contextual Influence Scaling (CIS) adjusts the FiT based on how closely the present demand and temperature match the maximum or minimum values of the recent time window. This part allows the FiT to be adjusted based on variations in demand and temperature from their two historical extreme conditions. The mathematical formulation of CIS is expressed as:

$$\text{CIS}(t) = b \cdot Fit_{max} \cdot \mathcal{S}(t) \quad (12)$$

Here, the scaling factor $S(t)$ aggregates the contextual influences from both demand and temperature at time t, defined as:

$$S(t) = \frac{S_D(t) + S_T(t)}{2} \tag{13}$$

The individual scaling functions $S_X(t)$, which handle the deviations of each input variable, are described as a piecewise function:

$$S_X(t) = \begin{cases} e^{\Psi_X^-(t)}, & \text{if } X(t) < \kappa_1 \cdot R_{\min}(X), \\ e^{\Psi_X^+(t)}, & \text{if } X(t) > \kappa_2 \cdot R_{\max}(X), \\ \Phi_X(t), & \text{otherwise,} \end{cases} \quad ; \quad X \in \{D, T\} \tag{14}$$

where the components are defined as:

$$\Psi_X^-(t) = \frac{\kappa_1 \cdot R_{\min}(X) - X(t)}{\Delta_X(t) + \epsilon} \tag{15}$$

$$\Psi_X^+(t) = \frac{X(t) - \kappa_2 \cdot R_{\max}(X)}{\Delta_X(t) + \epsilon} \tag{16}$$

$$\Phi_X(t) = \frac{|X(t) - \mu_X(t)|}{\Delta_X(t) + \epsilon} \tag{17}$$

here, κ_1 and κ_2 set thresholds for extreme deviations from the historical minimum and maximum of $X(t)$. When $X(t)$ falls below $\kappa_1 \cdot R_{\min}(X)$, $\Psi_X^-(t)$ amplifies the response through exponential divergence, while $\Psi_X^+(t)$ triggers exponential growth for values exceeding $\kappa_2 \cdot R_{\max}(X)$. In the intermediate range, $\Phi_X(t)$ employs a linear model centered at the midpoint ($\mu_X(t) = \frac{R_{\min}(X)+R_{\max}(X)}{2}$), normalized by the range ($\Delta_X(t) = R_{\max}(X) - R_{\min}(X)$).

The CIS part ensures that the FiT is sensitive to demand and temperature swings, capturing both severe and routine variations. Energy consumption increases with cooling demands on summer days and heating demands during colder months. The CIS component considers temperature-induced variations, prompting prosumers to sell excess energy during peak demand periods.

2.5. Dynamic Risk Adaptation (DRA)

The DRA component regulates the FiT to consider fast fluctuations in demand to enhance the system's adaptability to volatility. It employs a Generalized Autoregressive Conditional Heteroskedasticity (GARCH) model to calculate a dynamic weight ($\mathcal{DW}(t)$) that effectively measures and responds to time-varying changes (Gbolagade et al., 2022; Ayele et al., 2020). The following conditional expression represents the DRA contribution to the FiT:

$$\text{DRA}(t) = \begin{cases} c \cdot Fit_{max} \cdot \mathcal{DW}(t), & \text{if } \mathcal{V}_D(t) > \tau : \quad \mathcal{DW}(t) = \frac{\sigma_t}{\sigma_t + \epsilon} \\ 0, & \text{otherwise} \end{cases} \tag{18}$$

where $\mathcal{V}_D(t)$ is the demand volatility and σ_t represents the conditional volatility at time t which is calculated using a GARCH(5,5) model. ϵ is a small smoothing constant introduced to regulate sensitivity and prevent division by zero. The conditional volatility σ_t^2 is modeled by the GARCH(5,5) process as:

$$\sigma_t^2 = \omega + \sum_{i=1}^{5} \theta_i \cdot \mathcal{L}^i\left(v_t^2\right) + \sum_{j=1}^{5} \phi_j \cdot \mathcal{L}^j\left(\sigma_t^2\right) \tag{19}$$

where, ω is the long-term variance constant, θ_i is the impact of previous shocks, and v_{t-i}^2 is the squared residuals from time $t-i$. The lagged variances σ_{t-j}^2 model the persistence of previous variances shown by ϕ_j. The lag operator $\mathcal{L}$ captures recent and long-term volatility patterns by considering these previous dependencies. To compute demand volatility, we adapt the continuous-time approximation to a discrete form, given our 30-min interval data. Now, the $\mathcal{V}_D(t)$ over a specific time window Δt can be expressed as:

$$\mathcal{V}_D(t) = \frac{\sqrt{\frac{1}{N}\sum_{i=1}^{N}\left(D_i - \mu_D\right)^2}}{\mu_D} \quad : \quad \mu_D = \frac{1}{N}\sum_{i=1}^{N} D_i \tag{20}$$

where N is the number of intervals and μ_D is the mean demand in Δt time-frame. D_i is the demand value for every time stamp within the window, and $\left(D_i - \mu_D\right)^2$ measures the squared departures from the mean demand. The volatility metric is normalized by dividing by μ_D, similar to the standard deviation.

The FiT calculation's DRA component responds to the final tariff only on demand volatility, with temperature effects indirectly captured through fluctuations in demand. High demand fluctuation means that future demand might differ from predicted values and either go higher or lower than predictions. The DRA considers this by looking at past demand trends and using those patterns to predict future volatility. If previous demand patterns show much variation, the DRA incorporates an impact factor based on the level of previous demand volatility to its adjustment. This enables FiT to be sensitive to sudden demand variations.

The Sequential Model-Based Optimization (SMBO) algorithm determines the optimal weights in Eq. (9), enabling FiT to more effectively adapt to various input parameters, trends, and volatility. The goal is to optimize the weights ($\mathcal{W}_\alpha, \mathcal{W}_\beta, \mathcal{W}_\gamma, \mathcal{W}_{\alpha_1}, \mathcal{W}_{\beta_1}, \mathcal{W}_{\gamma_1}$) that influence the dominating part of FiT calculation. The optimization procedure creates a surrogate model by employing a Gaussian procedure (GP) to approximate the objective function successfully. After that, this GP model iteratively finds the most promising candidate spots to navigate the search for ideal weight values. The GP continuously improves its predictions to achieve the best potential outcomes by computing the posterior mean ($\mu_i(x)$) and variance ($\zeta_i^2(x)$) for any given set of weights at each step. The mathematical formulas to calculate $\mu_i(x)$ and $\zeta_i^2(x)$ are as follows:

$$\mu_i(x) = \sum_{k=1}^{n} \mathbf{k}_i(x, \mathbf{X}_k)\left(\mathbf{K}^{-1}\mathbf{y}\right)_k ; \quad x = (\mathcal{W}_\alpha, \mathcal{W}_\beta, \mathcal{W}_\gamma, \mathcal{W}_{\alpha_1}, \mathcal{W}_{\beta_1}, \mathcal{W}_{\gamma_1}) \tag{21}$$

$$\zeta_i^2(x) = k_i(x, x) - \sum_{k=1}^{n}\sum_{l=1}^{n} \mathbf{k}_i(x, \mathbf{X}_k)\left(\mathbf{K}_{kl}^{-1}\right)\mathbf{k}_l(x, \mathbf{X}_l) \tag{22}$$

The predicted mean $\mu_i(x)$ estimates the objective function's behavior for a given set of weight values. The term $\mathbf{k}_i(x, \mathbf{X}_k)$ represents the covariance between the test point x and previously observed data points $\mathbf{X}_k$, which makes sure that forecasts based on past evaluations are accurate in the future. The model is able to iteratively update its mean estimate using prior knowledge since the factor $(\mathbf{K}^{-1}\mathbf{y})_k$ takes into account the effect of observed function values $\mathbf{y}$. In Eq. (22), $\zeta_i^2(x)$ measures the prediction uncertainty at x. The first self-covariance is given by $k_i(x, x)$, and it is improved by the summing terms using data from the past. A high $\zeta_i^2(x)$ value suggests that there are unexplored regions, which guides the optimizer to sample additional points in order to enhance its predictions. The kernel function $\mathbf{K}(x, x')$ used to compute the covariance between points is defined as:

$$\mathbf{K}(x, x') = \zeta_f^2 \exp\left(-\frac{1}{2}\sum_{i=1}^{d}\sum_{j=1}^{d}(x_i - x_i')^\top \mathbf{L}_{ij}^{-1}(x_j - x_j') + p_{ij}(x_i - x_i')(x_j - x_j')\right) \tag{23}$$

The Gaussian Process model requires this kernel function to compare x and x'. The term ζ_f^2 adjusts covariance, and the exponential term makes sure correlation decreases with distance. The smoothness is regulated by the matrix $\mathbf{L}_{ij}^{-1}$ and the capacity to capture complex weight interactions is enhanced by the quadratic term $p_{ij}(x_i - x_i')(x_j - x_j')$. In the optimization process, an acquisition function determines the next evaluation point. A commonly utilized acquisition function is Expected Improvement (EI), defined as:

$$\begin{aligned} \alpha_{\text{EI}}(x) = &\sum_{i=1}^{n}\left(\sum_{k=1}^{n}\mathbf{k}_i(x, \mathbf{X}_k)\left(\mathbf{K}^{-1}\mathbf{y}\right)_k - \text{FiT}_{\text{best}}\right) \\ &\times \Phi\left(\frac{1}{\zeta_i(x)}\left(\sum_{k=1}^{n}\mathbf{k}_i(x, \mathbf{X}_k)\left(\mathbf{K}^{-1}\mathbf{y}\right)_k - \text{FiT}_{\text{best}}\right)\right) \\ &+ \sum_{j=1}^{n}\left(\zeta_j(x)\right)\phi\left(\frac{\sum_{k=1}^{n}\mathbf{k}_j(x, \mathbf{X}_k)\left(\mathbf{K}^{-1}\mathbf{y}\right)_k - \text{FiT}_{\text{best}}}{\sqrt{\zeta^2(x)}}\right) \end{aligned} \tag{24}$$

$$\frac{\partial \alpha_{\mathrm{EI}}(\mathcal{W})}{\partial \mathcal{W}_i} = \underbrace{\frac{\partial}{\partial \mathcal{W}_i}\left[\left(\sum_{k=1}^{n} \mathbf{k}_i(\mathcal{W}, \mathbf{X}_k)\left(\mathbf{K}^{-1}\mathbf{y}\right)_k - \mathrm{FiT}_{\mathrm{best}}\right)\Phi\left(\frac{\sum_{k=1}^{n} \mathbf{k}_i(\mathcal{W}, \mathbf{X}_k)\left(\mathbf{K}^{-1}\mathbf{y}\right)_k - \mathrm{FiT}_{\mathrm{best}}}{\sqrt{\zeta^2(\mathcal{W})}}\right)\right]}_{\text{Mean Component}} + \underbrace{\frac{\partial}{\partial \mathcal{W}_i}\left[\sqrt{\zeta^2(\mathcal{W})}\phi\left(\frac{\sum_{k=1}^{n} \mathbf{k}_i(\mathcal{W}, \mathbf{X}_k)\left(\mathbf{K}^{-1}\mathbf{y}\right)_k - \mathrm{FiT}_{\mathrm{best}}}{\sqrt{\zeta^2(\mathcal{W})}}\right)\right]}_{\text{Variance Component}} \tag{26}$$

Box I.

The EI function effectively balances exploration and exploitation during optimization. It analyzes prediction uncertainty and potential improvement over the best FiT value. The first term in Eq. (24) represents the predicted gain over $\mathrm{FiT}_{\mathrm{best}}$, weighted by $\Phi(.)$, while the second term integrates the standard deviation $\zeta(x)$ for assisting sampling in uncertain regions. Once the acquisition function has been evaluated, the next set of weights $\mathcal{W}_{\mathrm{next}}$ to explore is given by:

$$\mathcal{W}_{\mathrm{next}} = \arg\max_{\mathcal{W}} \left[\sum_{i=1}^{n} \mathbf{k}_i(\mathcal{W}, \mathbf{X}_k)\left(\mathbf{K}^{-1}\mathbf{y}\right)_k + \kappa\sqrt{\sum_{j=1}^{n} \mathbf{k}_j(\mathcal{W}, \mathbf{X}_k)\mathbf{K}^{-1}\mathbf{k}_j(\mathcal{W}, \mathbf{X}_k)}\right] \tag{25}$$

The gradients of the $\alpha_{\mathrm{EI}}(x)$ with respect to each of the six weights $(\mathcal{W}_\alpha, \mathcal{W}_\beta, \mathcal{W}_\gamma, \mathcal{W}_{\alpha_1}, \mathcal{W}_{\beta_1}, \mathcal{W}_{\gamma_1})$ must be computed in order to accomplish effective optimization. These gradients balance the mean and variance of the acquisition function during optimization. The EI acquisition function gradient is: (see the Eq. (26) in Box I).

Using the gradient of the EI function for each weight parameter $\mathcal{W}_i$, the optimization method can identify the best route for improving FiT. It has two basic components. The mean component reflects the impact of changes in $\mathcal{W}_i$ on predicted improvement over the best-known FiT value. This term uses the probability function $\Phi(.)$ to rank promising search space locations. A standard deviation $\zeta(\mathcal{W})$ and a probability density function $\phi(.)$ are used in the variance component to account for uncertainty. This prevents the optimizer from getting stuck in local optima by encouraging exploration in unexplored regions. Finally, the posterior covariance matrix encapsulates the correlation between the assessed weights $\mathcal{W}_i$ and $\mathcal{W}_j$, defined as:

$$\mathbf{K}(\mathcal{W}_i, \mathcal{W}_j) = \zeta_f^2 \exp\left\{-\frac{1}{2}\sum_{p=1}^{d}\sum_{q=1}^{d}(\mathcal{W}_{i,p} - \mathcal{W}_{j,p})^{\top}\mathbf{L}_{pq}^{-1}(\mathcal{W}_{i,q} - \mathcal{W}_{j,q}) + p_{pq}(\mathcal{W}_{i,p} - \mathcal{W}_{j,p})(\mathcal{W}_{i,q} - \mathcal{W}_{j,q})\right\} + \zeta_n^2\delta_{ij} \tag{27}$$

The previous step's posterior covariance matrix captures the relationships between the evaluated weight configurations and indicates their influence on the goal outcome. The algorithm iteratively optimizes weights by choosing configurations that maximize $\alpha_{\mathrm{EI}}(x)$, based on parameters $\mu_i(x)$ and $\zeta_i^2(x)$. This method ensures that each iteration approaches closer to the optimal weight settings in response to fluctuations in input parameters and trends. Algorithm 1 outlines the full SMBO process for this search for ideal weights.

Algorithm 1 Sequential Model-Based Optimization algorithm for FiT Calculation

Initialize: Define initial dataset $\mathcal{D}_0 = \{(\mathcal{W}_i, \mathrm{FiT}(\mathcal{W}_i))\}_{i=1}^{n}$ with initial weight samples $\mathcal{W}_i$.
Set: Surrogate model $\mathbf{K}(\mathcal{W}_i, \mathcal{W}_j)$ with hyperparameters ζ_f^2 and ζ_n^2, acquisition function $\alpha_{\mathrm{EI}}(\mathcal{W})$, and iteration limit T.
for $t = 1$ to T **do**
  Step 1: Update Posterior
  Calculate posterior mean and variance for $\mathcal{W}$:

$$\mu_t(\mathcal{W}) = \sum_{k=1}^{n} \mathbf{k}_i(\mathcal{W}, \mathbf{X}_k)\left(\mathbf{K}^{-1}\mathbf{y}\right)_k$$

$$\zeta_t^2(\mathcal{W}) = k_i(\mathcal{W}, \mathcal{W}) - \sum_{k=1}^{n}\sum_{l=1}^{n} \mathbf{k}_i(\mathcal{W}, \mathbf{X}_k)\left(\mathbf{K}_{kl}^{-1}\right)\mathbf{k}_l(\mathcal{W}, \mathbf{X}_l)$$

  Step 2: Optimize Acquisition Function
  Solve:

$$\mathcal{W}_{\mathrm{next}} = \arg\max_{\mathcal{W}} \alpha_{\mathrm{EI}}(\mathcal{W}) = \arg\max_{\mathcal{W}} \left[\mu_t(\mathcal{W}) + \kappa\zeta_t(\mathcal{W})\right]$$

  Step 3: Evaluate Objective Function
  Compute $\mathrm{FiT}(\mathcal{W}_{\mathrm{next}})$ and add to dataset: $\mathcal{D}_{t+1} = \mathcal{D}_t \cup \{(\mathcal{W}_{\mathrm{next}}, \mathrm{FiT}(\mathcal{W}_{\mathrm{next}}))\}$.
  Step 4: Update Model
  Update $\mathbf{K}(\mathcal{W}_i, \mathcal{W}_j)$ with new data point $\mathcal{W}_{\mathrm{next}}$.
  if convergence criterion is met **then**
    Break
  end if
end for
Output: Optimal weight configuration $\mathcal{W}^* = \arg\max_{\mathcal{W}\in\mathcal{D}_T} \mathrm{FiT}(\mathcal{W})$.

Following the computation of FiT using optimal weights and inputs, this study applies Distance Correlation to determine the correlation coefficient, which assesses the degree of relationship between FiT and each input. A non-linear correlation coefficient technique is implemented to capture these complex dependencies accurately, as both the inputs and outputs are non-linear. Additionally, Permutation Importance analysis reveals the individual impacts of each input. The mathematical expressions for these metrics are provided in the following discussions.

Distance Correlation

Distance Correlation (DC) is a statistical metric that assesses both linear and non-linear relationships between variables (Edelmann et al., 2021; Martínez-Gómez et al., 2014). DC is employed in this study to represent the relationship between each of the input variables D, PV, and T and the calculated FiT. For two random vectors X and Y, where $X = \{D, PV, T\}$ and $Y = \mathrm{FiT}$, the distance covariance, $\mathcal{V}(X, Y)$, is calculated as follows:

$$\mathcal{V}^2(X, Y) = \frac{1}{n^2}\sum_{i=1}^{n}\sum_{j=1}^{n} d_X(i, j)\cdot d_Y(i, j) \tag{28}$$

where $d_X(i, j) = |D_i - D_j| + |PV_i - PV_j| + |T_i - T_j|$ and $d_Y(i, j) = |\mathrm{FiT}_i - \mathrm{FiT}_j|$ represent pairwise Euclidean distances for X and Y, respectively. The distance correlation coefficient, $\mathcal{R}_{\mathrm{Dist}}(X, Y)$, is then

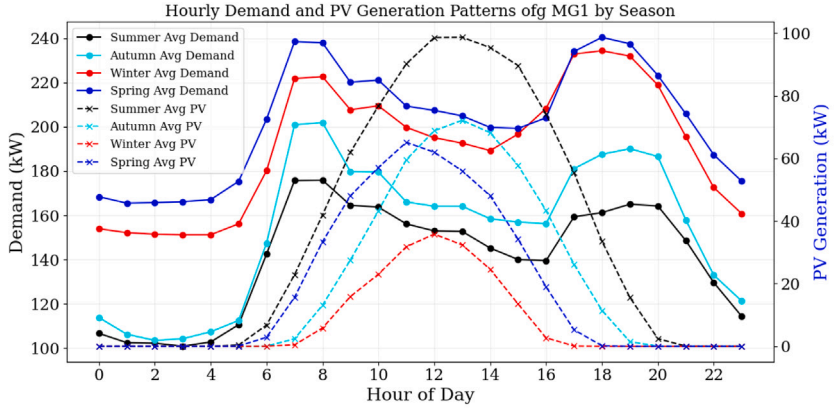

(a) MG1 profile

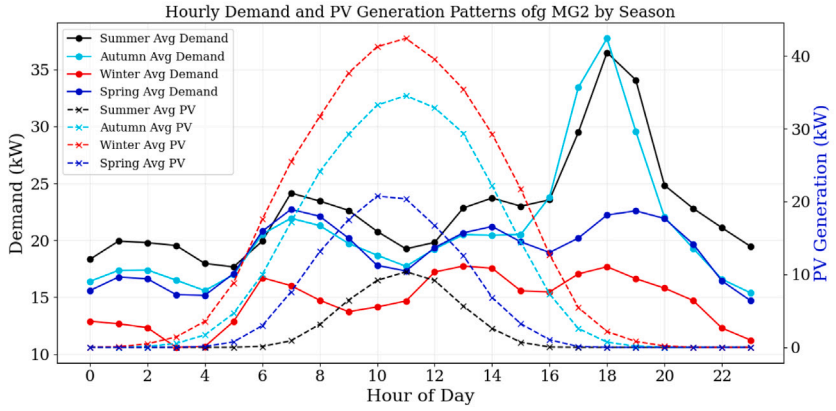

(b) MG2 profile

Fig. 2. Electricity demand and PV generation profiles of two Australian microgrids.

defined as:

$$\mathcal{R}_{\text{Dist}}(X,Y) = \frac{\mathcal{V}(X,Y)}{\sqrt{\mathcal{V}(X,X)\cdot\mathcal{V}(Y,Y)}} \tag{29}$$

The coefficient ranges from 0 to 1, where 0 indicates 'independence' and 1 signifies 'perfect dependence.' It assesses both linear and nonlinear relationships between FiT and the input factors.

Permutation Importance

Permutation Importance (PI) evaluates each feature's impact on model accuracy by measuring the decrease in accuracy when the feature's relationship with the target is interrupted. For a model $f(X)$ trained on dataset $D = \{(X_i, y_i)\}_{i=1}^{n}$, where $X = \{D, PV, T\}$ represents the input features and y = FiT the target, the permutation importance $\mathcal{I}_{\text{perm}}(X_j)$ for feature X_j is defined as (Huang et al., 2016; Kaneko, 2022):

$$\mathcal{I}_{\text{perm}}(X_j) = \mathbb{E}_{\pi}\left[\frac{1}{n}\sum_{i=1}^{n}\left(f(X_{\pi,-j}) - f(X_{-j})\right)^2\right] \tag{30}$$

where $X_{\pi,-j}$ represents the original dataset without permuting X_j, and X_{-j} represents the dataset with feature X_j disrupted (permuted) according to permutation π. The average squared difference in model predictions due to disruption of X_j is quantified to determine its impact on the target.

In summary, the proposed dynamic FiT system integrates historical and predicted data on demand, PV generation, and temperature to account for both long-term trends and real-time variations. This flexible framework is built on three key components. First, primary trend contribution identifies whether these factors are increasing or decreasing, enabling the FiT to adjust accordingly. Second, contextual influence scaling (CIS) fine-tunes the tariff under both normal and extreme conditions by comparing current temperature and demand against recent extremes. Third, dynamic risk adaptation (DRA) employs a GARCH-based method to manage unexpected demand fluctuations. Finally, sequential model-based optimization iteratively tests different weighting scenarios to achieve an optimal balance among these components, ensuring fast and reliable FiT calculations.

3. Results and discussions

In this study, two Australian microgrids from New South Wales (NSW) region are studied, labeled MG1 and MG2, and the average demand and PV generation are shown in Fig. 2. The two microgrids were chosen to validate the performance of the proposed model under various scenarios. The MG1 is a typical microgrid with a peak demand greater than the maximum green energy generation. Conversely, the residents of MG2 installed a more significant percentage of PV, resulting in a peak PV generation greater than the peak average demand. Figs. 2(a) and 2(b) show the average demand and PV generation for all four seasons in Australia: summer (January, February, December), autumn (March-May), winter (June-August), and spring (September-November).

The summer, autumn, and winter data of MG1 are utilized as Cases 1, 2, and 3, respectively. MG2's data was used in Cases 4 and 5 with two distinct PV-demand scenarios. Case 4 considers the days with a high PV generation and an abrupt demand surge in the late afternoon, while Case 5 considers the fluctuating PV generation with almost equal demand throughout the day, with typical fluctuations. The proposed model is highly adaptable across different regions, as

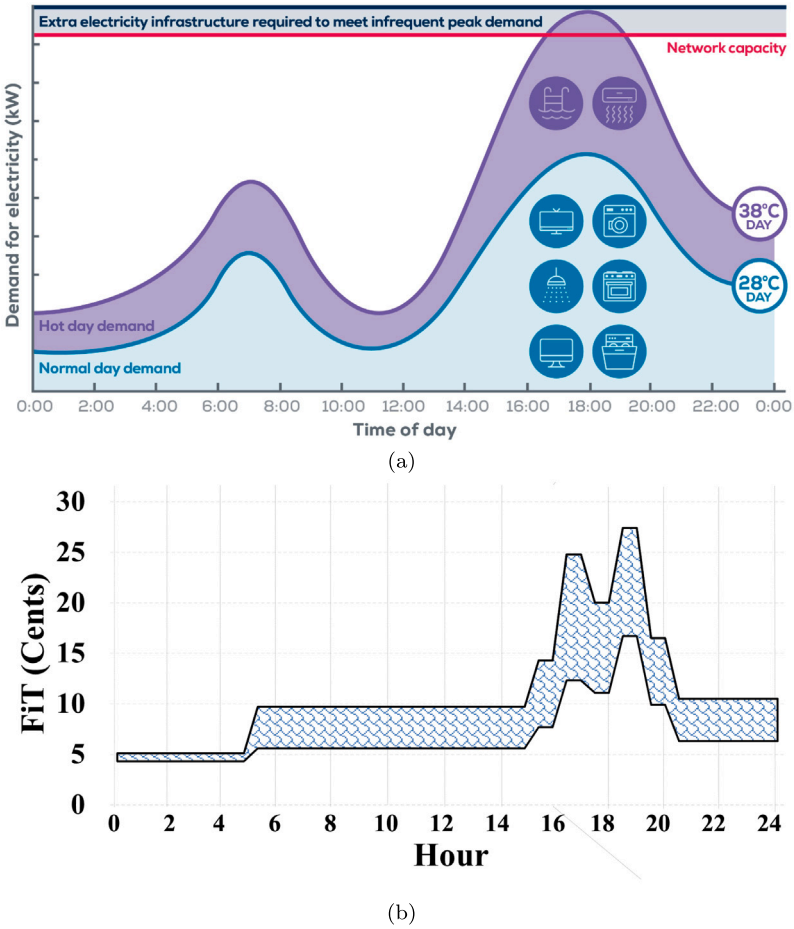

Fig. 3. (a) Typical electricity demand profile in Australia (Endeavour Energy, 2024) and (b) FiT range applied in case studies.

it operates independently of location-specific parameters or regulatory constraints. It can be applied to any microgrid or distributed energy system using only historical and predicted demand, PV generation, temperature, and region-specific FiT regulations.

The FiT range used in this study is set by the NSW state government and adjusted annually based on previous market dynamics and new capacity installations, export percentage at different times and other similar factors (IPART NSW, 2024). Fig. 3(a) depicts Australia's typical electricity consumption patterns during both average and hot days, showing that load demand remains relatively stable from midnight to 5 AM before fluctuating throughout the day (Endeavour Energy, 2024). The government's minimum FiT trading value is considered during this early morning period (IPART NSW, 2021). A variable FiT range is then implemented for the rest of the day to respond to changing demand levels (IPART NSW, 2023). On hot days, demand is at its highest in the late afternoon and evening when there is little to no PV power. In NSW, sunset typically occurs between 7:30 and 8:00 PM during daylight saving time, partially aligning with early peak demand. However, in winter, the sun may set as early as 5:00 PM, well before the typical peak from 6:00 to 8:00 PM. This timing challenge highlights the importance of a flexible FiT structure that incentivizes energy exports or storage in the evening. To address this, prosumers receive a higher rate when solar output declines, as shown in Figure 3b. The tariff is designed to peak during these hours, allowing green energy producers to maximize profits by selling surplus solar or stored energy when grid demand is highest. The framework encourages prosumers to export energy during these high-demand, low-renewable generation periods by offering a higher FiT. This modified FiT strategy, illustrated in Fig. 3(b), supports government objectives by promoting energy exports during critical demand times. The effectiveness of the proposed FiT model is assessed in the case studies according to various energy scenarios. Based on demand, PV production, and temperature changes, each case looks at how the model dynamically changes tariffs.

Several case studies are conducted to validate the efficacy of the proposed FiT model. Case Study 1 examines scenarios where high demand exceeds PV generation, while Case Study 2 analyzes both consistent and variable PV generation profiles during peak demand periods. Case Study 3 explores minimal PV generation with steady demand, Case Study 4 assesses low daytime demand with spikes in the evening, and Case Study 5 considers stable demand alongside fluctuating PV generation. These scenarios serve to validate the model's adaptability to variations in input parameters.

3.1. Case study 1

This case study assesses the effectiveness of the proposed FiT in both typical PV generation patterns and variable PV profiles, which show distinct peaks and valleys during periods of high demand and low PV generation. Based on MG1's summer season data, Fig. 4 illustrates the FiT profile over two days. In Fig. 4(a), the FiT demonstrates a nearly symmetrical response to demand fluctuations. Following a lower peak demand the previous day, the FiT reaches the peak export rate shortly after 5 a.m. with a slight increase in demand. The FiT decreases between 10 a.m. and 1 p.m. as demand drops and PV generation rises, and vice versa. In the late afternoon, as solar output and demand decline, the FiT rapidly falls, reflecting reduced power export necessity. On the second day (Fig. 4(b)), the FiT gradually rises after 5 a.m. in response to increased demand. By 1 p.m., with a decrease in PV

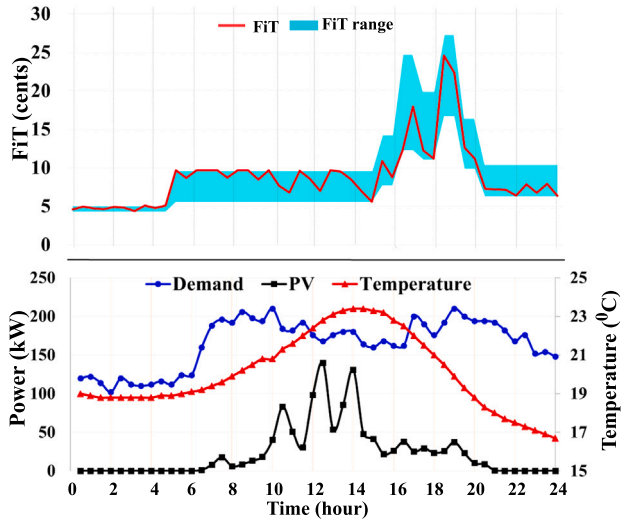

(a) Day 1

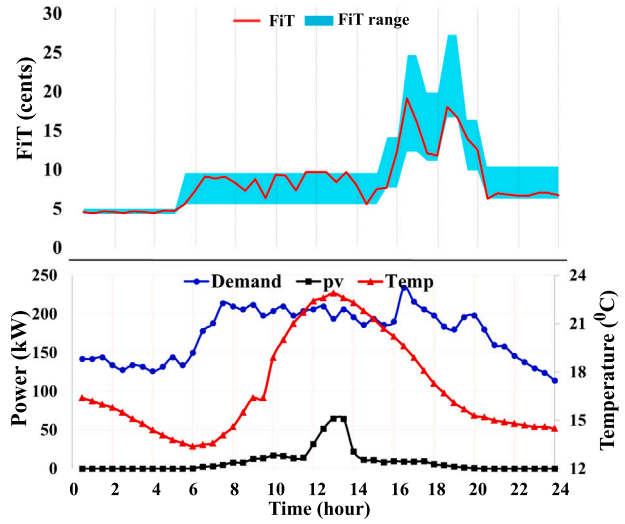

(b) Day 2

Fig. 4. (a) Demand, PV generation, and Temperature profile with FiT for Case Study 1, Day 1, and (b) corresponding profiles and FiT for Day 2.

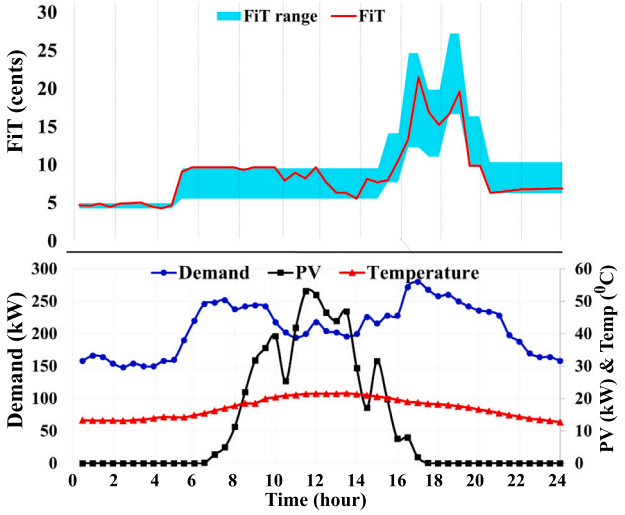

(a) Day 1

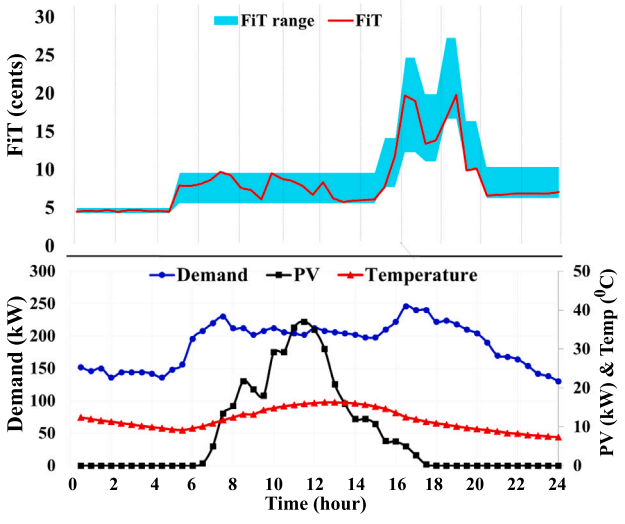

(b) Day 2

Fig. 5. Daily profiles for Case Study 2: (a) Demand, PV generation, Temperature, and FiT on Day 1, and (b) the same variables on Day 2.

generation, demand, and temperature, the FiT drops from its maximum to its minimum rate. Subsequently, as demand shows two minor peaks, the FiT trend rises as expected. Overall, the calculated FiT aligns with the expected output. This scenario shows the FiT model's ability to modify tariffs to change demand patterns.

3.2. Case study 2

This case study evaluates the adaptability of the proposed FiT in conditions with both stable and fluctuating PV generation, especially when peak generation coincides with daily peak demand. Fig. 5 presents the FiT profile for MG1 over two autumn days. In Fig. 5(a), demand rises sharply from 5 a.m., causing the FiT to peak in this period. As observed in Case Study 1, the FiT fluctuates between 9 a.m. and 2 p.m. Demand declines gradually from 11 a.m. to 2 p.m., while PV generation decreases after peaking once during this interval, resulting in the FiT dropping from its peak to its lowest level. Afterward, the FiT climbs sharply as demand rises and PV generation declines.

However, after 5 p.m., demand steadily decreases until midnight, and the FiT mirrors this downward trend. A similar PV generation and demand pattern on the second day causes the FiT to follow a similar trajectory, highlighting the interaction between generation and consumption. This scenario underscores the FiT model's sensitivity to PV generation variability, ensuring that tariff adjustments align with fluctuations in renewable output.

3.3. Case study 3

Case Study 3 aims to evaluate the impact of PV generation volume on the proposed FiT, given this minimal generation compared to previous cases. Fig. 6 depicts the FiT profile on winter days for MG1, which has the lowest PV generation. On Day 1, (Fig. 6(a)) and 2 (Fig. 6(b)), PV generation fluctuates, peaking around 10 a.m., while demand remains mostly steady. This results in a dip in the FiT during those times. In the afternoon, as PV generation decreases, a minor increase in demand occurs due to falling temperatures, leading to a sharp rise in the FiT. Peak demand occurs on Day 1 at 6:30 p.m. and on Day 2 at 5 p.m.,

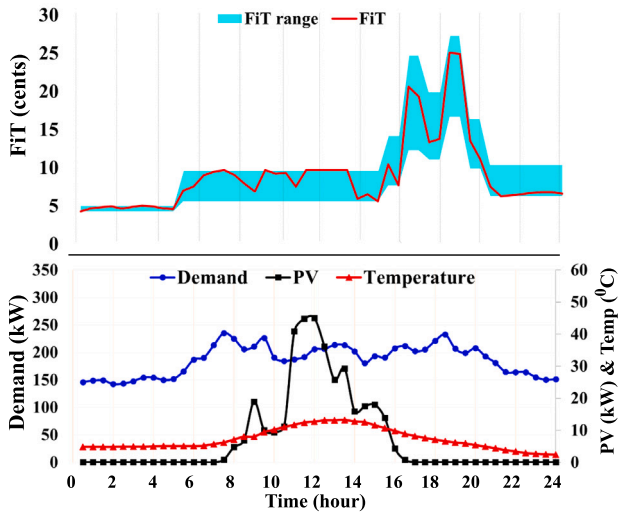

(a) Day 1

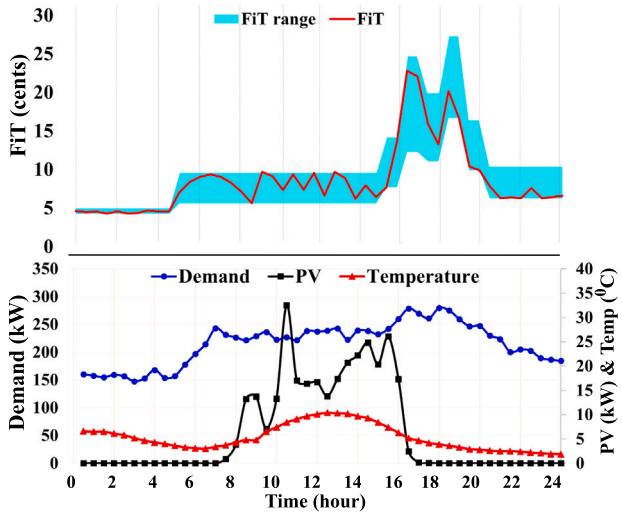

(b) Day 2

Fig. 6. Graphical depiction of Demand, PV generation, Temperature, and the computed FiT derived from these variables for (a) Case Study 3, Day 1, and (b) Case Study 3, Day 2.

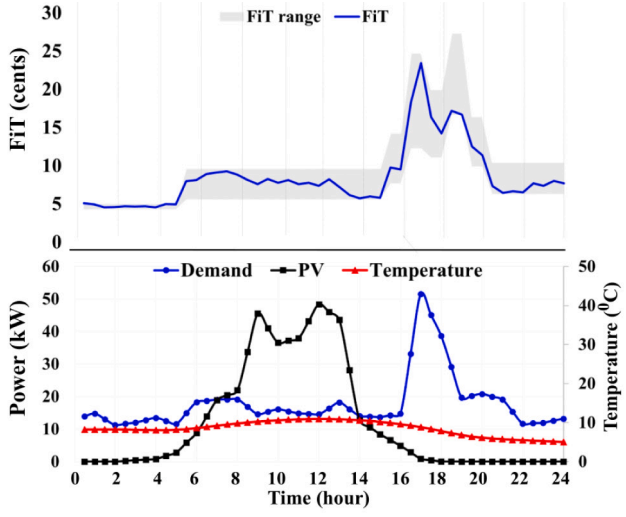

(a) Day 1

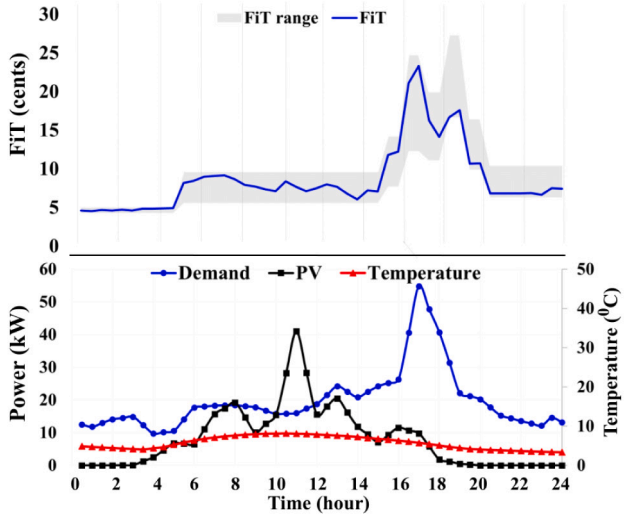

(b) Day 2

Fig. 7. Visual representation of the calculated FiT, PV generation, temperature, and demand for (a) Case study 4 day 1 and (b) Case study 4 day 2.

aligning with each day's highest FiT values. Variations in temperature, relatively stable demand, and fluctuating PV generation significantly shape FiT patterns throughout both days. This scenario highlights the FiT model's sensitivity to low PV generation and temperature-driven demand changes, ensuring tariffs align with environmental and demand factors.

3.4. Case study 4

This case study aims to evaluate the performance of the proposed FiT model in response to a sudden demand increase. The analysis for Case Study 4 utilizes MG2 data from days characterized by low daytime demand and high PV generation, followed by a significant demand surge in the evening. Figs. 7(a) and 7(b) illustrate the FiT profiles for two similar types of days. On Day 1, as PV generation begins, demand also rises, causing the FiT to increase accordingly. After 7 a.m., PV generation surpasses demand and remains higher until 2 p.m., during which the FiT fluctuates but stays below the morning level. Following 2 p.m., demand stabilizes at levels similar to those from 9 a.m. to 12 p.m., while a gradual decline in PV generation raises the FiT slightly. A notable increase in the FiT occurs as demand rises quickly and PV generation drops after 4 p.m. Both demand and the FiT gradually decrease from 7 p.m. to 10 p.m.; however, after 10 p.m., the FiT rises again as demand increases. Similar trends are observed in the FiT pattern on Day 2 in Fig. 7(b), where the FiT reaches its peak during periods of high demand relative to PV generation. This scenario demonstrates that the FiT model effectively adjusts tariffs to reflect sudden demand surges.

3.5. Case study 5

In this case study, the performance of the FiT model is evaluated under conditions of standard daily demand fluctuations and variable PV generation. The FiT profile of MG2 for two days is depicted in Fig. 8. On the first day (Fig. 8(a)), PV generation reaches the peak demand level, whereas on the second day (Fig. 8(b)), the peak PV generation surpasses demand. Demand and PV generation fluctuate during Day 1, which

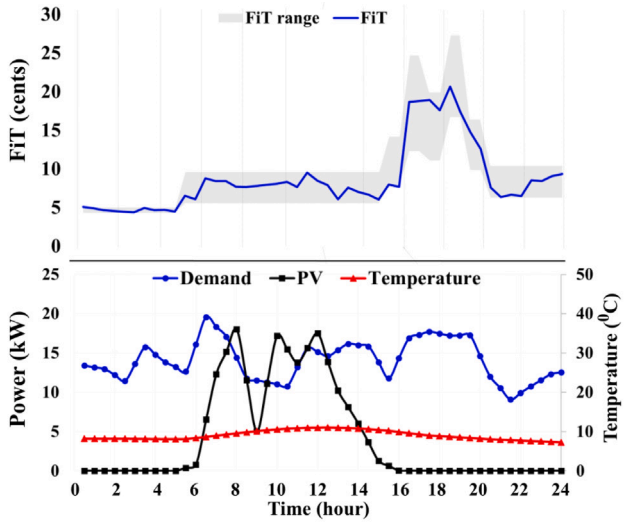

(a) Day 1

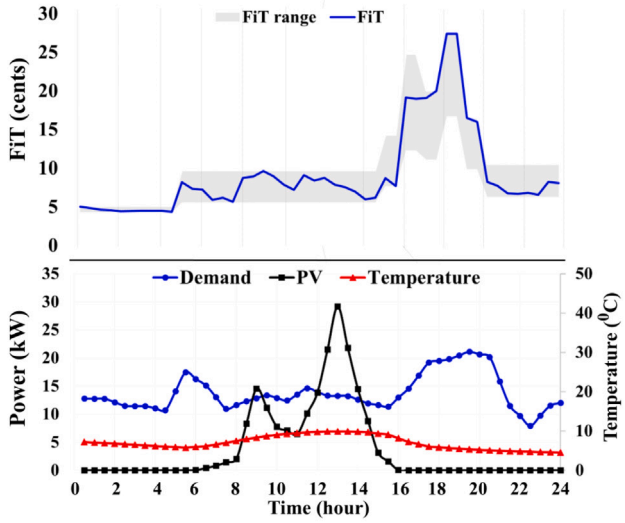

(b) Day 2

Fig. 8. Daily profiles for Case Study 5: (a) Demand, PV generation, temperature, and FiT on Day 1, and (b) the same variables on Day 2.

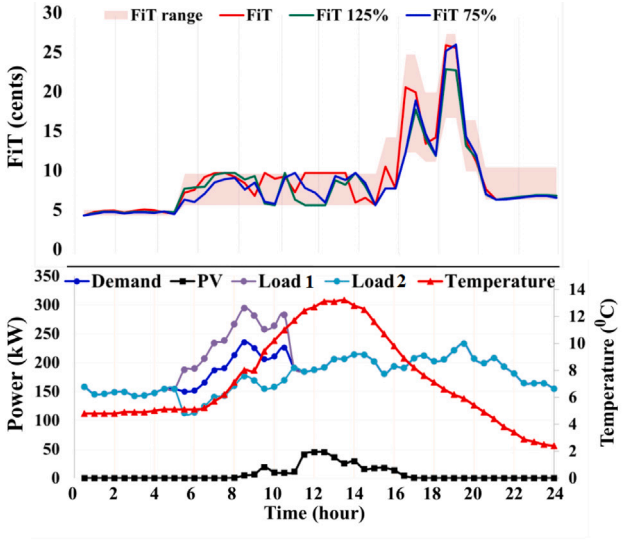

(a) Day 1

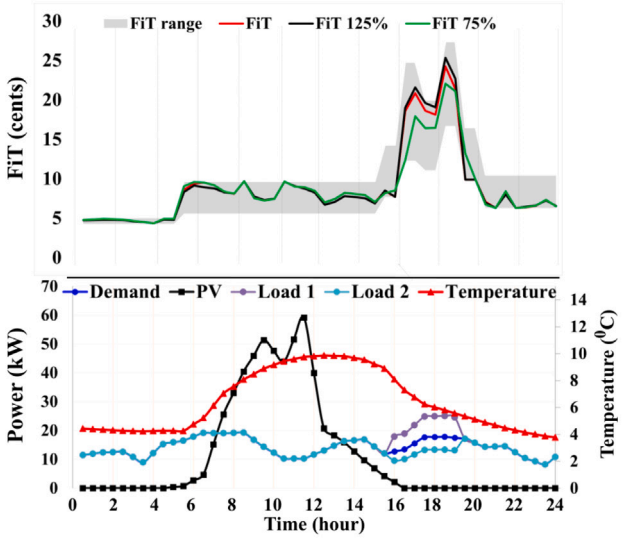

(b) Day 2

Fig. 9. (a) Demand, PV generation, temperature, and calculated FiT for MG1 with ±25% demand variation in the early morning; (b) corresponding plot for MG2 with ±25% demand variation in the afternoon.

causes FiT also to fluctuate. Demand experiences an initial decline after 2 p.m., followed by a rapid increase, which remains consistent until approximately 7:30 p.m., and FiT reflects these fluctuations.

Following this period, demand falls below the previous day's minimum, causing the FiT to reach its lowest level. As shown in Fig. 8(b), demand then rises sharply after 4 p.m., exceeding the peak demand level of the previous day. Consequently, the FiT reaches a high point during this time before decreasing as demand tapers off. This pattern demonstrates the FiT model's responsiveness to changes in demand and PV generation. The model's sensitivity to fluctuations in PV generation enables adaptive tariff adjustments under varying generation conditions.

3.6. Sensitivity analysis

The sensitivity analysis of the calculated FiT in response to variations in demand for MG1 and MG2 is depicted in Figs. 9(a) and 9(b). This study examines how the performance of the FiT algorithm changes with a single input parameter at different times of day, while other factors remain constant. The ±25% increased and decreased load from the actual demand are termed Load 1 and Load 2, respectively. As illustrated in Fig. 9(a), a demand shift between 5 and 11 a.m. significantly affects FiT, while PV generation and Temperature remain unchanged. Demand reductions lead to the lowest FiT until 10:30 a.m., with a peak at 11 a.m. aligning with maximum daytime demand. If demand exceeds previous peaks, FiT also reaches the peak of that time, reflecting the sensitivity to these variations. FiT reaches its daily maximum at 7 p.m., however peak demand at 7:30 p.m. does not result in the highest rate due to a drop in temperature. In scenarios of 25% enhanced demand, FiT reaches its maximum at 7 a.m., while the nighttime FiT is the lowest of the three scenarios due to the most significant decrease in demand compared to the daytime peaks. Fig. 9(b) illustrates similar tendencies in the FiT for MG2 data. The FiT for the Load 1 profile is lower than the other two profiles due to a smaller proportion of demand. However, it slightly surpasses the FiT for the actual demand

Load 2's at the end of the considered period due to the upward trend. In contrast, the FiT for Load 2 consistently exceeds the actual demand as a result of a continuous upward trend, reaching its maximum within the analyzed past window. This analysis demonstrates that the proposed FiT adequately captures demand variation.

3.7. Results analysis

Fig. 10 represents the SMBO algorithm's convergence behavior in five case studies, with and without PV generation (when PV < 2 kW) data. The x-axis represents the number of iterations, while the y-axis shows the RMSE (Root Mean Square Error) value. Case studies with PV data are shown in Fig. 10(a), where the RMSE values start with higher variability and exhibit notable variations within the first iterations. The optimization process converges as iterations increase, as evidenced by the gradual stabilization of each example, with RMSE attaining a lower and constant value between 60 and 70 iterations. Despite the early instability brought on by the increased complexity of PV generation data, this convergence trend with PV data indicates that the algorithm successfully minimizes error. A similar convergence pattern, albeit with fewer initial fluctuations, is seen in the second graph (Fig. 10(b)), which depicts case studies without PV data. Each case achieves a steady, reduced RMSE value after about 30 repetitions, demonstrating faster convergence than the cases with PV data. The optimization process is simplified by the absence of PV generation, which enables the algorithm to attain a stable error level more rapidly. In conclusion, the optimization process effectively converges both scenarios, precisely minimizing RMSE to ensure consistent error levels across all case studies. The convergence plot is shown in Fig. 10.

The statistical results of PI and DC analysis for five cases using MG1 and MG2 data are shown in Fig. 11, which shows an evident influence of each input on the FiT value. In the PI analysis (Fig. 11(a)), the bar heights show the feature importance values for each parameter over all five scenarios. In contrast, the values at the bottom of each bar represent the standard deviation. PV always has the most significant feature importance in the PI analysis (except for Case 4), which means it significantly affects the FiT calculation. Demand and Temperature also play a role, but less so. In the Distance Correlation analysis (Fig. 11(b)), FiT significantly correlates with Demand, PV, and Temperature, with Demand typically showing the strongest correlation. This combination of correlation and importance analysis emphasizes the relevance of each parameter in accurately computing FiT results. It confirms that Fit is sensitive to modifications in every input feature.

The efficiency of the SMBO optimization method is now compared to other popular algorithms such as Particle Swarm Optimization (PSO) (Zaini et al., 2023), Teaching Learning Optimization (TLBO) (Zhou et al., 2023), and Genetic method (GA) (Alhijawi and Awajan, 2024). Table 3 displays the optimal fitness value and computational time for a single iteration. According to the statistics, GA and TLBO take a lot more time per iteration because they have two stages: selection and crossover in GA and teacher-learner phases in TLBO. These phases involve extensive computation for each individual in the population, which is responsible for the longer elapsed time. Even though PSO is quicker than GA and TLBO, it still takes a long time because it iteratively updates particle velocities and locations while maintaining boundaries and inertia weight modifications. On the other hand, SMBO optimizes the objective function using a surrogate model, which significantly cuts down on computation time without sacrificing accuracy. This result highlights that the proposed framework can provide optimized FiT rates quicker than other algorithms with superior computational efficiency.

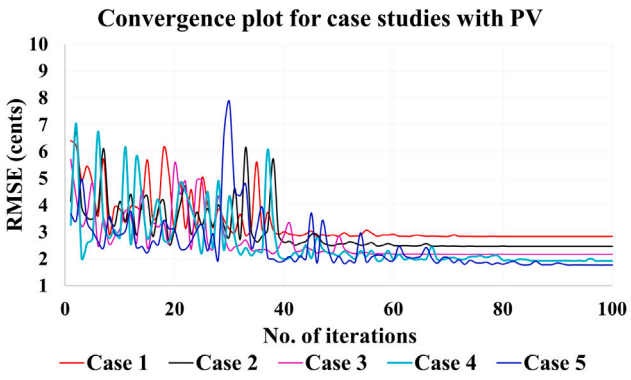

(a) Day 1

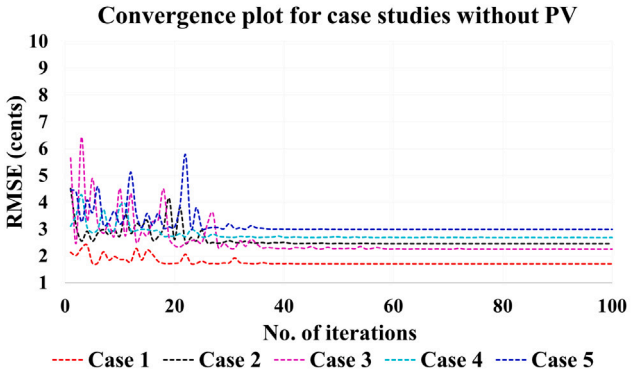

(b) Day 2

Fig. 10. Convergence plot of optimization algorithm for different cases with (a) PV generation and (b) without PV generation.

Table 3
Comparison of optimization algorithms regarding best fitness and average time elapsed for a single iteration.

	PSO	TLBO	GA	SMBO
Best fitness (RMSE)	3.078	2.902	2.849	2.839
Time (minutes)	25	28	35	2.05

3.8. Economic benefit and payback analysis

This case study evaluates the financial impacts of the proposed DFiT and TOU pricing for three randomly selected MG1 customers: a household with a 10-kWh battery (R1), a house without a battery (R2), and a small industrial consumer with a 40-kWh battery (R3). Fig. 12 illustrates their daily consumption patterns over two consecutive days. The analysis examines how these pricing schemes influence electricity costs, export revenues, and the benefits of battery storage.

Table 4 compares export revenues under the dynamic FiT, which fluctuates based on various input factors, to a fixed FiT of 6 cents per kilowatt-hour. On Day 1, R1 earns $3.55 with the dynamic FiT but only $2.10 with the fixed FiT; R2 makes $2.62 under the dynamic FiT compared to $1.55 with the fixed FiT; and R3 generates $10.51 instead of $6.23. A similar pattern is observed on Day 2, confirming that the dynamic FiT provides higher earnings for prosumers.

The second scenario examines how battery storage impacts revenue and electricity costs for prosumers using batteries. Unlike the initial scenario, where all photovoltaic generation was immediately exported, this case allows prosumers to store energy before using surplus power. Residential TOU rates for R1 and R2 are 57.78 ¢/kWh during peak hours (2 PM–8 PM), 29.83 ¢/kWh during shoulder hours (7 AM–2

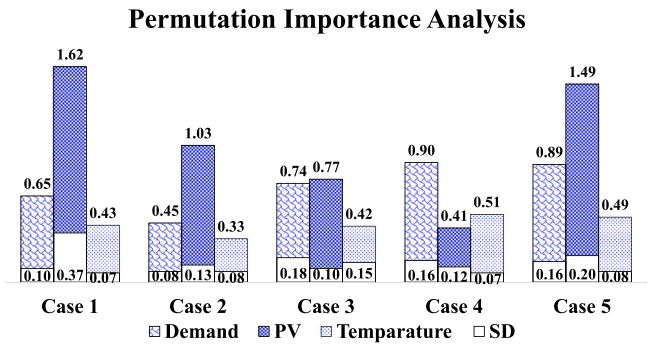

(a) Permutation Importance analysis

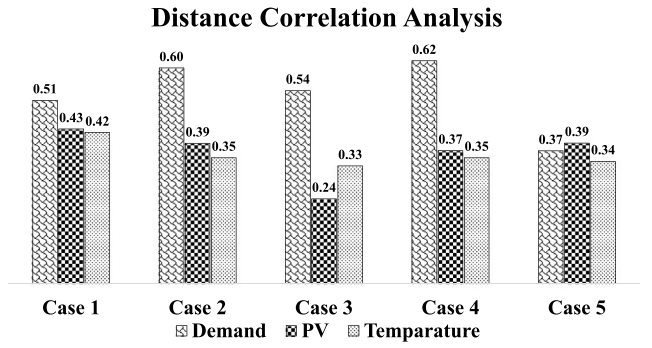

(b) Distance Correlation analysis

Fig. 11. Analysis of the impact of input feature strength with the FiT through Permutation Importance and Distance Correlation.

Table 4
Comparison of earnings with dynamic FiT and fixed FiT.

Consumer	Day 1			Day 2		
	Earnings ($)		Savings ($)	Earnings ($)		Savings ($)
	DFiT	FFiT		DFiT	FFiT	
R1	3.55	2.10	1.45	3.39	2.14	1.25
R2	2.63	1.56	1.07	2.51	1.59	0.92
R3	10.51	6.23	4.28	10.04	6.35	3.69

PM, 8 PM–10 PM), and 22.42 ¢/kWh during off-peak hours (10 PM–7 AM). For small industrial consumers (R3), the rates are 60.64 ¢/kWh, 30.60 ¢/kWh, and 21.13 ¢/kWh, respectively (AGL Energy, 2023). When storage reaches its maximum capacity (10 kWh for R1 and 40 kWh for R3), any excess energy is used immediately. After 6 p.m., when export rates are higher, R1 and R3 discharge their stored energy and export it at government-set limits (5 kWh/h for R1 and 10 kWh/h for R3) to maximize earnings.

As shown in Table 5, battery storage combined with the dynamic FiT significantly enhances financial benefits. "TOU Cost (Pre-Export)" represents electricity costs under TOU rates without PV generation, while "TOU Cost (Post-Export)" reflects the final cost after selling stored energy to the grid, as outlined in the second scenario.

On Day 1, R1's earnings increase from $3.55 to $5.94, reducing their total bill from $9.04 to $3.10. R3's earnings rise from $10.51 to $14.78, lowering their bill from $251.13 to $236.35. A similar trend occurs on Day 2, with R1's earnings growing from $3.39 to $5.62, decreasing their bill from $13.38 to $7.76, while R3's profits increase to $14.32, reducing their bill from $231.92 to $217.60.

R2, without a battery, benefits only from self-consumption and solar exports but does not gain additional savings from energy storage.

The payback period analysis demonstrates that implementing the DFiT alongside battery storage offers a financial advantage. For R1, who has a 10-kWh battery, the average daily earnings without storage are $3.47, leading to an annual income of $1267. Although the battery installation costs $13,900 (Solar Choice, 2024), using battery storage increases daily earnings by $1.35, adding $492.75 to annual revenue. As a result, the payback period, including the cost of the PV system, is reduced from 11 years under a fixed FiT to 9.22 years under DFiT.

Similarly, for R2, who does not have a battery, the average daily savings from DFiT over a fixed FiT is $0.99, totaling $361.35 annually. This reduces R2's payback period from 9.5 years under a fixed FiT to 8.5 years under DFiT.

For R3, who has a 40-kWh battery, direct PV generation exports to the grid yield an average daily earning of $10.28, resulting in an annual income of $3753. With an estimated $41,700 battery installation cost and an additional $4.23 per day from battery storage, R3 earns an extra $1544 annually. The overall payback period drops from 11.12 years under a fixed FiT to 9.20 years under DFiT.

These results demonstrate that DFiT significantly improves the financial viability of battery storage and renewable energy investments by substantially reducing the payback period for prosumers.

Table 5
Impact of battery storage and dynamic FiT on earnings and electricity bills.

Consumer	Day	Earnings ($)		Total bill ($)		
		No battery	With battery	Fixed tariff	TOU cost pre-export	TOU cost post-export
R1	Day 1	3.55	5.94	9.89	9.04	3.10
R1	Day 2	3.39	5.62	11.62	13.38	7.76
R2	Day 1	2.63	–	19.65	22.70	20.07
R2	Day 2	2.51	–	10.05	8.34	5.83
R3	Day 1	10.51	14.78	307.59	251.13	236.35
R3	Day 2	10.04	14.32	283.80	231.92	217.60

4. Limitations of this research

The proposed DFiT model provides significant benefits for prosumers by enhancing financial returns and optimizing energy management through market-driven pricing. Its flexibility ensures fair compensation and reduced payback periods. However, there are limitations to consider. While the dynamic FiT structure promotes equitable pricing, benefits may vary among solar generators due to differences in generation capacity and cost structures. The framework focuses solely on PV incentives, excluding other renewable sources like wind, hydrogen, and tidal energy. Additionally, the study does not explore how export rates and energy exchanges can be coordinated across multiple microgrids, which represents a crucial area for future research. As solar technology advances and costs decrease, newer prosumers with more efficient devices may have an advantage in revenue generation compared to early adopters with older technology. This study does not account for this potential profitability gap and its long-term implications for existing prosumers.

5. Conclusion and future research direction

This study introduces a data-driven framework for dynamic FiT computation that adapts to the inherent variability in renewable energy production and customer demand. The dynamic FiT model in this study aligns with IPART's annual standards, ensuring prosumers receive a guaranteed minimum rate while offering higher returns during peak demand. This framework reduces financial risks and enhances confidence for both prosumers and lenders by establishing regulated limits. By analyzing historical data on demand, solar generation, and temperature, the model accurately reflects input parameter fluctuations, ensuring that FiT values align with real-world conditions. The SMBO optimization algorithm enhances the influence of input factors, enabling the FiT computation to respond effectively to both short-term

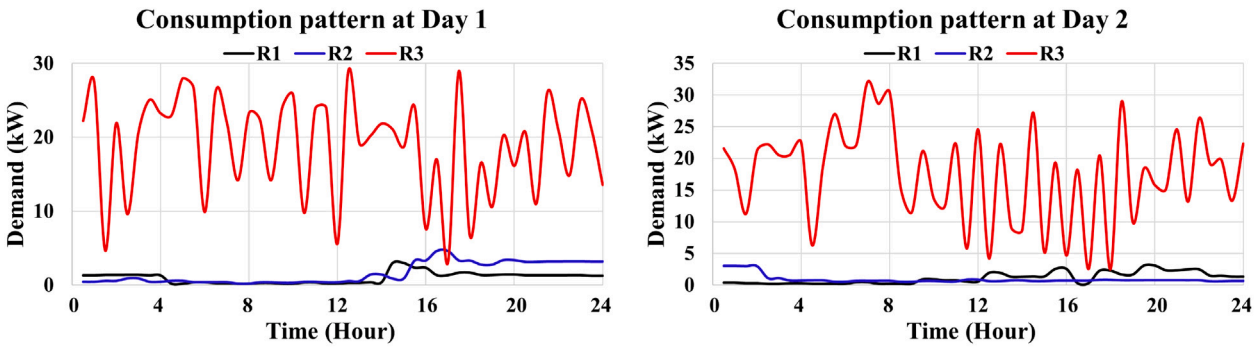

(a) Consumption pattern for Day 1

(b) Consumption pattern for Day 2

Fig. 12. Two consecutive day's consumption pattern for R1, R2, and R3.

changes and long-term trends. Case studies using real data demonstrate the model's flexibility and confirm that the computed FiT values remain within predefined limits. The DFiT model enhances fairness by linking prosumer income to the retailer's variable pricing, ensuring that incentives align with real-time demand instead of a static rate. Furthermore, prosumers with battery storage can earn more than those without by selling energy during peak price periods, which contributes to a fairer system for all. The framework's adaptability and rapid calculation make it suitable for real-time applications in dynamic energy markets, offering an alternative to static export tariffs. As renewable energy adoption increases, the proposed model's capability to deliver fair and optimized tariffs supports global sustainability goals, fostering a more resilient and eco-friendly energy ecosystem.

Future research could enhance the model by integrating uncertainty quantification to manage unexpected variations in renewable generation and demand. The FiT model can incorporate probabilistic forecasts and dynamically adjust tariffs based on real-time confidence intervals by using Monte Carlo simulations or Bayesian optimization. Applying probabilistic modeling or robust optimization techniques would enable the framework to better respond to rapid demand surges and extreme weather conditions, significantly affecting FiT calculations. A hybrid optimization strategy combining robust optimization and reinforcement learning can also be considered for dynamically fine-tuning the FiT pricing. Short-term market responsiveness and long-term policy goals can be balanced utilizing the updated framework. Future research could examine FiT structures for prosumers' changing investment costs and technology. Tiered dynamic FiT systems depending on system age, efficiency, and original investment could fairly compensate early adopters and newcomers. Furthermore, customized FiT models for various prosumer groups, such as small residential and large industrial producers, could boost market competitiveness.

Advanced machine learning techniques, such as Long Short-Term Memory (LSTM) networks and autoencoders, can be leveraged to detect and remove anomalies in historical and predicted data in real time. This could enhance the accuracy and reliability of calculated FiT values, leading to more stable and fair pricing. Future research can assess the framework using comprehensive datasets from diverse geographical regions, grid conditions, and market structures to validate its scalability and robustness. Additionally, aligning the dynamic FiT model with evolving regulatory frameworks is crucial. Future studies can explore collaborations with policymakers to integrate this model into grid pricing schemes, fostering market stability and consumer confidence. These advancements will further improve the adaptability and real-world applicability of the proposed FiT computation framework.

CRediT authorship contribution statement

Md. Ahasan Habib: Writing – original draft, Visualization, Validation, Methodology, Investigation, Formal analysis, Data curation, Conceptualization. **M.J. Hossain:** Writing – review & editing, Supervision, Software, Resources, Project administration.

Declaration of competing interest

The authors declare that they have no known competing financial interests or personal relationships that could have appeared to influence the work reported in this paper.

Data availability

Data will be made available on request.

References

AGL Energy, 2023. AGL NSW electricity standing offer prices - july 2023. URL https://www.agl.com.au/content/dam/digital/agl/documents/terms-and-conditions/energy/rates-and-contracts/standard-retail-contracts/nsw/agl-nsw-electricity-standing-offer-prices-july-2023.pdf. (Accessed 27 February 2024).

Alhijawi, B., Awajan, A., 2024. Genetic algorithms: Theory, genetic operators, solutions, and applications. Evol. Intell. 17 (3), 1245–1256.

Alizamir, S., de Véricourt, F., Sun, P., 2016. Efficient feed-in-tariff policies for renewable energy technologies. Oper. Res. 64 (1), 52–66.

Auffhammer, M., Wang, M., Xie, L., Xu, J., 2021. Renewable electricity development in China: Policies, performance, and challenges. Rev. Environ. Econ. Policy 15 (2), 323–339.

2024. Small-scale renewable energy scheme. https://cer.gov.au/schemes/renewable-energy-target/small-scale-renewable-energy-scheme. (Accessed 13 June 2024).

2024. Feed-in tariffs: State by state. https://www.energycouncil.com.au/media/12974/feed-in-tariffs-state-by-state.pdf. (Accessed 03 October 2024).

Ayele, A.W., Gabreyohannes, E., Edmealem, H., 2020. Generalized autoregressive conditional heteroskedastic model to examine silver price volatility and its macroeconomic determinant in Ethiopia market. J. Probab. Stat. 2020 (1), 5095181.

Azhgaliyeva, D., Le, H., Olivares, R.O., Tian, S., 2024. Renewable energy investments and feed-in tariffs: firm-level evidence from Southeast Asia. Appl. Energy 374, 123986.

Balta-Ozkan, N., Yildirim, J., Connor, P.M., Truckell, I., Hart, P., 2021. Energy transition at local level: Analyzing the role of peer effects and socio-economic factors on UK solar photovoltaic deployment. Energy Policy 148, 112004.

Cai, Q., Qing, J., Xu, Q., Shi, G., Liang, Q.-M., 2024. Techno-economic impact of electricity price mechanism and demand response on residential rooftop photovoltaic integration. Renew. Sustain. Energy Rev. 189, 113964.

2024. China added more solar panels in 2023 than US did in its entire history. https://www.carbonbrief.org/daily-brief/china-added-more-solar-panels-in-2023-than-us-did-in-its-entire-history. (Accessed 03 October 2024).

Castaneda, M., Zapata, S., Cherni, J., Aristizabal, A.J., Dyner, I., 2020. The long-term effects of cautious feed-in tariff reductions on photovoltaic generation in the UK residential sector. Renew. Energy 155, 1432–1443.

2024. How China became the world's leader on renewable energy. URL https://e360.yale.edu/features/china-renewable-energy. (Accessed 20 June 2024).

Clean Energy Council, 2024. Clean energy Australia report 2024. URL https://cleanenergycouncil.org.au/getmedia/0cb12425-37ab-479e-9a4b-529622cc9c02/clean-energy-australia-2024.pdf. (Accessed 27 February 2024).

Dato, P., Durmaz, T., Pommeret, A., 2021. Feed-in tariff policy in Hong Kong: Is it efficient? City Environ. Interact. 10, 100056.

Dobrowolski, Z., Drozdowski, G., 2022. Does the net present value as a financial metric fit investment in green energy security? Energies 15 (1), 353.

Edelmann, D., Móri, T.F., Székely, G.J., 2021. On relationships between the Pearson and the distance correlation coefficients. Statist. Probab. Lett. 169, 108960.
Endeavour Energy, 2024. How to save energy: Peak demand. URL https://www.endeavourenergy.com.au/your-energy/how-to-save-energy/peak-demand. (Accessed 30 October 2024).
2024. Renewable energy in India. https://www.investindia.gov.in/sector/renewable-energy#:~:text=India's%20installed%20non%2Dfossil%20fuel,additions%20of%209.83%25%20in%202022. (Accessed 03 October 2024).
2024. Federal solar tax credits for businesses. https://www.energy.gov/eere/solar/federal-solar-tax-credits-businesses#_edn1. (Accessed 13 June 2024).
Feng, K., Chang, R.-D., Wang, Y., Zuo, J., Yang, C., Shan, M., Gao, B., Goodsite, M., 2023. Low-income and elderly with feed-in tariffs drive solar installation rates for energy equity.
Gbolagade, S., Oyeyemi, G., Abidoye, A., Adejumo, T., Okegbade, A., 2022. Performance of generalized autoregressive conditional heteroscedasticity (GARCH) models in modeling volatility of brent crude oil price. Ilorin J. Sci. 9 (1), 20–32.
Gholami, H., Nils Røstvik, H., 2021. Levelised cost of electricity (LCOE) of building integrated photovoltaics (BIPV) in Europe, rational feed-in tariffs and subsidies. Energies 14 (9), 2531.
Górnowicz, R., Castro, R., 2020. Optimal design and economic analysis of a PV system operating under net metering or feed-in-tariff support mechanisms: A case study in Poland. Sustain. Energy Technol. Assess. 42, 100863.
Hackbarth, A., Löbbe, S., 2020. Attitudes, preferences, and intentions of German households concerning participation in peer-to-peer electricity trading. Energy Policy 138, 111238.
Huang, N., Lu, G., Xu, D., 2016. A permutation importance-based feature selection method for short-term electricity load forecasting using random forest. Energies 9 (10), 767.
2024. Renewable energy support policies in europe. https://climatepolicyinfohub.eu/renewable-energy-support-policies-europe.html. (Accessed 05 October 2024).
IPART NSW, 2021. Final report: Solar feed-in tariffs benchmarks 2021-22. URL https://www.ipart.nsw.gov.au/sites/default/files/cm9_documents/Final-Report-Solar-feed-in-tariffs-benchmarks-2021-22-June-2021.PDF. (Accessed 30 October 2024).
IPART NSW, 2023. Fact sheet: Time-of-day solar feed-in tariff benchmarks 2023-24. URL https://www.ipart.nsw.gov.au/sites/default/files/cm9_documents/Fact-Sheet-Time-of-day-solar-feed-in-tariff-benchmarks-2023-24-28-April-2023.PDF. (Accessed 30 October 2024).
IPART NSW, 2024. Solar energy - retail prices. URL https://www.ipart.nsw.gov.au/Home/Industries/Energy/Retail-prices/Solar-Energy. (Accessed 30 October 2024).
Kabir, M.A., Farjana, F., Choudhury, R., Kayes, A.I., Ali, M.S., Farrok, O., 2023. Net-metering and feed-in-tariff policies for the optimum billing scheme for future industrial PV systems in Bangladesh. Alex. Eng. J. 63, 157–174.
Kaneko, H., 2022. Cross-validated permutation feature importance considering correlation between features. Anal. Sci. Adv. 3 (9–10), 278–287.
Kimura, K., Lundberg, L., Kåberger, T., 2025. How high feed-in tariffs impacted the capital cost of solar PV in Japan. Renew. Energy 122685.
Kurbatova, T., Sotnyk, I., Prokopenko, O., Bashynska, I., Pysmenna, U., 2023. Improving the feed-in tariff policy for renewable energy promotion in Ukraine's households. Energies 16 (19), 6773.
Le, H.T.-T., Sanseverino, E.R., Nguyen, D.-Q., Di Silvestre, M.L., Favuzza, S., Pham, M.-H., 2022. Critical assessment of feed-in tariffs and solar photovoltaic development in Vietnam. Energies 15 (2), 556.
Lewis, M., 2023. The first of China's desert solar and wind projects is online, and it's huge. URL https://electrek.co/2023/04/28/chinas-solar-wind-desert/. (Accessed 20 June 2024).
Li, L., Liu, J., Zhu, L., Zhang, X.-B., 2020. How to design a dynamic feed-in tariffs mechanism for renewables–a real options approach. Int. J. Prod. Res. 58 (14), 4352–4366.
Li, H.X., Zhang, Y., Li, Y., Huang, J., Costin, G., Zhang, P., 2021. Exploring payback-year based feed-in tariff mechanisms in Australia. Energy Policy 150, 112133.
Lin, B., Chen, Y., 2023. Impact of the feed-in tariff policy on renewable innovation: evidence from wind power industry and photovoltaic power industry in China. Energy J. 44 (2), 29–46.
Lin, B., Xie, Y., 2024. How feed-in-tariff subsidies affect renewable energy investments in China? New evidence from firm-level data. Energy 294, 130853.
Ma, R., Cai, H., Ji, Q., Zhai, P., 2021. The impact of feed-in tariff degression on R&D investment in renewable energy: The case of the solar PV industry. Energy Policy 151, 112209.
le Maitre, J., 2024. Price or public participation? Community benefits for onshore wind in Ireland, Denmark, Germany and the United Kingdom. Energy Res. Soc. Sci. 114, 103605.
Martínez-Gómez, E., Richards, M.T., Richards, D.S.P., 2014. Distance correlation methods for discovering associations in large astrophysical databases. Astrophys. J. 781 (1), 39.
Nagata, T., Arino, Y., Nakano, Y., Akimoto, K., 2018. Assessment of equity of feed-in tariff in Japan. In: 2018 International Conference and Utility Exhibition on Green Energy for Sustainable Development. ICUE, IEEE, pp. 1–5.
2024. Solar bonus scheme review 2014. https://www.parliament.nsw.gov.au/tp/files/15731/Solar%20Bonus%20Scheme%20Review%202014.pdf. (Accessed 03 October 2024).
Ravichandran, D., Selvaraj, J., 2021. Study on the success and limitations of feed in tariff (fit) mechanism in Malaysia. Int. J. Renew. Energy Resour. 11 (2), 44–56.
Sagulpongmalee, K., Therdyothin, A., Nathakaranakule, A., 2019. Analysis of feed-in tariff models for photovoltaic systems in Thailand: An evidence-based approach. J. Renew. Sustain. Energy 11 (4).
Selinger-Lutz, O., Groß, A., Wille-Haussmann, B., Wittwer, C., 2020. Dynamic feed-in tariffs with reduced complexity and their impact on the optimal operation of a combined heat and power plant. Int. J. Electr. Power Energy Syst. 118, 105770.
Sener, C., Fthenakis, V., 2014. Energy policy and financing options to achieve solar energy grid penetration targets: Accounting for external costs. Renew. Sustain. Energy Rev. 32, 854–868.
Seyedzahedi, A., Bahramara, S., 2023. Facilitating investment in photovoltaic systems in Iran considering time-of-use feed-in-tariff and carbon market. Energies 16 (3), 1067.
Solar Choice, 2024. Solar battery prices in Australia. URL https://www.solarchoice.net.au/solar-batteries/price/. (Accessed 27 February 2024).
Sovacool, B.K., Barnacle, M.L., Smith, A., Brisbois, M.C., 2022. Towards improved solar energy justice: Exploring the complex inequities of household adoption of photovoltaic panels. Energy Policy 164, 112868.
Trends, G., 2017. Challenges and opportunities in the implementation of the sustainable development goals. U. N. Dev. Programme U. N. Res. Inst. Soc. Dev..
2024. Smart export guarantee (SEG) - contacts, guidance, and resources. https://www.ofgem.gov.uk/environmental-and-social-schemes/smart-export-guarantee-seg/smart-export-guarantee-seg-contacts-guidance-and-resources. (Accessed 13 June 2024).
2024. Victorian DER marketplace trial funded as grid integration blueprint. URL https://www.pv-magazine-australia.com/2020/12/02/victorian-der-marketplace-trial-funded-as-blueprint-for-widespread-grid-integration/. (Accessed 05 October 2024).
2024. Variable feed-in rates and VPPs in NSW. https://www.penrithsolar.com.au/blog/variable-feed-in-rates-and-vpps-in-nsw/. (Accessed 03 October 2024).
Wang, R., Hsu, S.-C., Zheng, S., Chen, J.-H., Li, X.I., 2020. Renewable energy microgrids: Economic evaluation and decision making for government policies to contribute to affordable and clean energy. Appl. Energy 274, 115287.
Yang, C., Ge, Z., 2018. Dynamic feed-in tariff pricing model of distributed photovoltaic generation in China. Energy Procedia 152, 27–32.
Yang, X., Matsumoto, S., 2023. To use or not to use, that is the question: Income and substitution effects in the feed-in tariff system for solar-generated electricity. Jpn. World Econ. 68, 101211.
Zaini, F.A., Sulaima, M.F., Razak, I.A.W.A., Zulkafli, N.I., Mokhlis, H., 2023. A review on the applications of PSO-based algorithm in demand side management: challenges and opportunities. IEEE Access 11, 53373–53400.
Zhang, L., Chen, C., Wang, Q., Zhou, D., 2021. The impact of feed-in tariff reduction and renewable portfolio standard on the development of distributed photovoltaic generation in China. Energy 232, 120933.
Zhang, A.H., Sirin, S.M., Fan, C., Bu, M., 2022. An analysis of the factors driving utility-scale solar PV investments in China: How effective was the feed-in tariff policy? Energy Policy 167, 113044.
Zhou, G., Zhou, Y., Deng, W., Yin, S., Zhang, Y., 2023. Advances in teaching-learning-based optimization algorithm: A comprehensive survey. Neurocomputing 126898.